Southeastern Geology: Volume 31, No. 1 June 1990

Edited by: S. Duncan Heron, Jr.

Abstract

Academic journal published quarterly by the Department of Geology, Duke University.

SOUTHEASTERN GEOLOGY

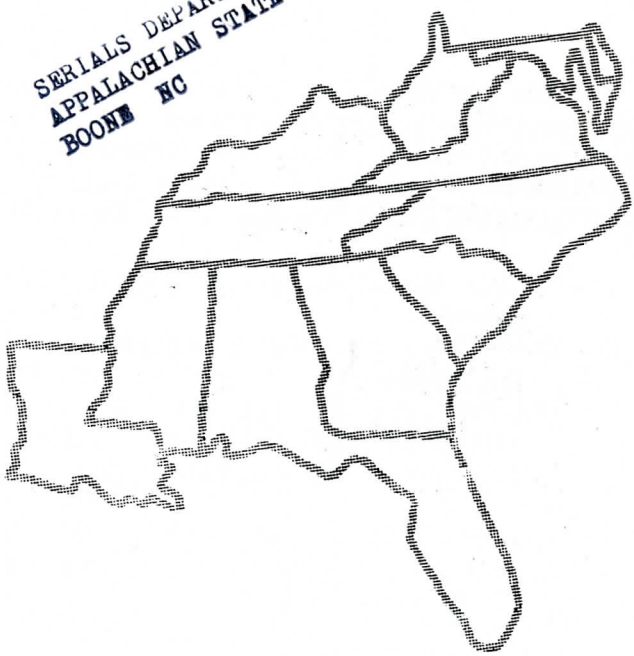

PUBLISHED AT DUKE UNIVERSITY DURHAM, NORTH CAROLINA

VOL. 31, NO. 1 JUNE 1990

SOUTHEASTERN GEOLOGY

PUBLISHED

AT

DUKE UNIVERSITY

Editor in Chief:
S. Duncan Heron, Jr.

Managing Editor:
James W. Clarke

This journal publishes the results of original research on all phases of geology, geophysics and geochemistry as related to the Southeast. Send manuscripts to **S. DUNCAN HERON, JR., DUKE UNIVERSITY, DEPARTMENT OF GEOLOGY, OLD CHEMISTRY BUILDING, DURHAM, NORTH CAROLINA 27706.** Observe the following:

1) Type the manuscript with double space lines and submit in duplicate.
2) Cite references and prepare bibliographic lists in accordance with the method found within the pages of this journal.
3) Submit line drawings and complex tables reduced to final publication size (no bigger than 8 x 5 1/8 inches).
4) Make certain that all photographs are sharp, clear, and of good contrast.
5) Stratigraphic terminology should abide by the North American Stratigraphic Code (Am. Assoc. Petroleum Geologists Bulletin, v. 67, p. 841-875).

Subscriptions to *Southeastern Geology* are $12.00 per volume (US and Canada), $16.00 per volume (foreign). Inquires should be sent to: **SOUTHEASTERN GEOLOGY, DUKE UNIVERSITY, DEPARTMENT OF GEOLOGY, OLD CHEMISTRY BUILDING, DURHAM, NORTH CAROLINA 27706.** Make checks payable to: *Southeastern Geology*.

ISSN 0038-3678

SOUTHEASTERN GEOLOGY

Table of Contents

Vol. 31, No. 1

June 1990

OCCURRENCE AND SIGNIFICANCE OF A ZONED HALLOYSITE (10A) AND ALLOPHANE DEPOSIT BELOW DEVONIAN BLACK SHALES IN CENTRAL KENTUCKY

F. R. ETTENSOHN

M. R. BAYAN

Department of Geological Sciences
University of Kentucky
Lexington, KY 40506-0059

ABSTRACT

Halloysite (10A) and allophane are major constituents in a lithologically and mineralogically zoned sequence that developed in residual Devonian-age calcareous physilites unconformably underlying the New Albany black shale in central Kentucky. The zonation seems to reflect the processes that resulted in halloysite and allophane formation. The basic alteration processes require a source of sulfuric acid and silica, the New Albany Shale, and result in an interval of silica enrichment, the halloysite zone, as well as an underlying interval of relative silica depletion, the allophane zone. Halloysite seems to have formed where the Si concentration of percolating solutions exceeded a threshold value. Dissolution of silicates in black-shale constituents provided enough excess silica to surpass this value in zones within residual clays immediately below the New Albany. The resulting precipitation of halloysite (10A) apparently depleted the silica and lowered the Si/Al ratio to the point that only allophane could form in the subjacent zone.

Any situation where pyritic sediments overlie silica-rich, calcareous deposits on unconformities may provide the potential for halloysite and allophane formation.

INTRODUCTION

Halloysite is a phyllosilicate more commonly associated with felsic volcanic terrains (e.g., Wada, 1977; Kirkman, 1981; Nagasawa and Noro, 1987) than it is with areas of Lower and Middle Paleozoic shales and carbonates as in central Kentucky. Yet in central Kentucky, prominent layers of white, plastic to porcelaneous halloysite, greater than a meter thick in places, was reported within the Paleozoic sequence by Crawford and McGrain in 1963. Because of the contrast between the white clays and overlying black Devonian shales, these deposits were noted very soon after the initial roadcuts were made (Rice, 1962). The position of the clays below the black shales led Rice (1962) to assume that they were somehow related to the overlying shales, but the clay minerals were very different compared to the typical sub-black-shale residua already known (Milton and others, 1955; Conant and Swanson, 1961). Not until analyses by Crawford and McGrain (1963) and later descriptions by Keller and others (1963), McGrain (1966, 1979) and McGrain and Kendall (1972) was it realized, however, that the clays were largely composed of halloysite. Halloysite is commonly associated with a non-crystalline phase like allophane (e.g., Ross and Kerr, 1934; Wada, 1977), and Keller and others (1966) similarly reported a non-crystalline phase underlying the central

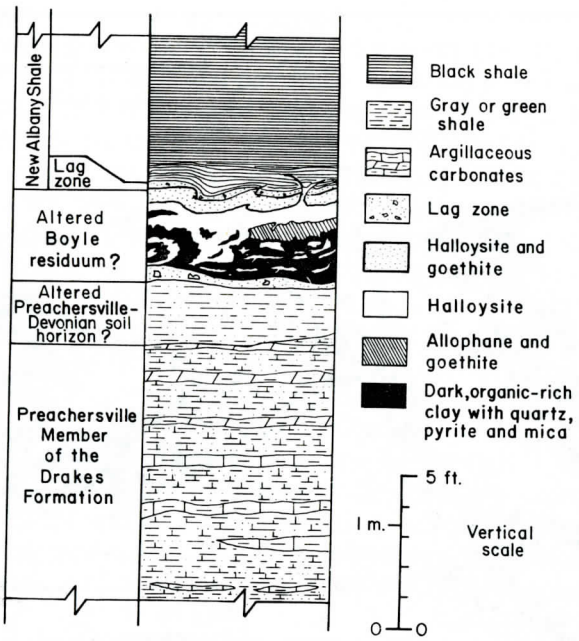

Figure 2. Schematic stratigraphic column of the studied section.

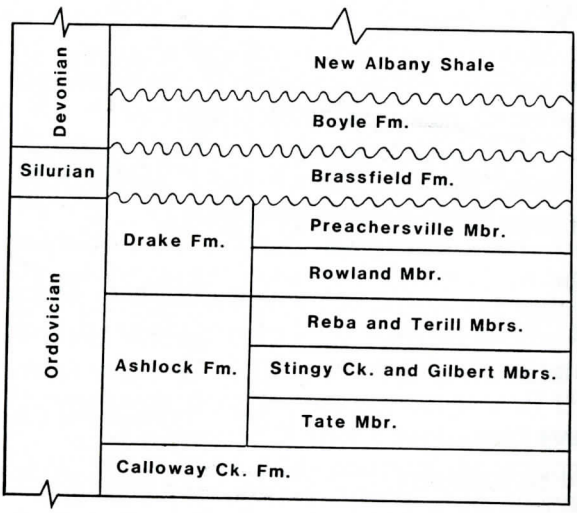

Figure 3. The normal stratigraphic sequence of lower and middle Paleozoic units in the study area. Irregular lines represent unconformable contacts.

The Middle Devonian Boyle Formation consists largely of cherty dolostones and minor carbonaceous shale (Shawe and Wigley, 1974) and is normally found disconformably overlying the Brassfield or younger Silurian formations (Figure 3).

North and west of the unnamed fault system, the Brassfield is absent and the Boyle may disconformably overlie Upper Ordovician units as old as the Stingy Creek and Gilbert members of the Ashlock Formation (Shawe and Wigley, 1974) (Figure 4). Within and just south of the unnamed fault system, the Boyle is absent so that the overlying New Albany Shale unconformably overlies Silurian or

Ordovician formations (Figure 4). However, a few kilometers south of this fault system, drilling records indicate that the Boyle Formation reappears and thickens to the south (Wilson and Sutton, 1973).

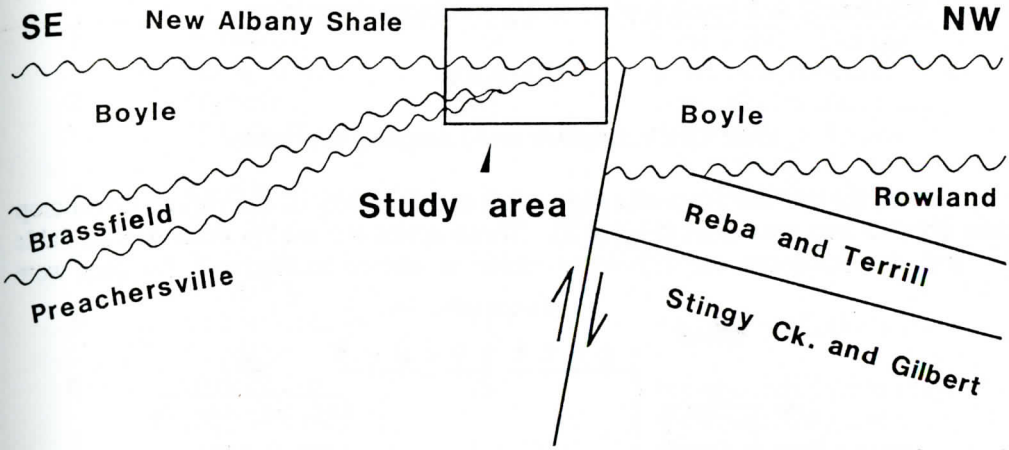

Figure 4. Schematic diagram showing the actual disposition of units and unconformities relative to structure in the immediate study area.

The New Albany Shale consists of pyritic Upper Devonian black shales; these shales unconformably overlie formations varying in age from Late Ordovician to Middle Devonian. Locally in the area, the lowest parts of the New Albany contain a breccia unit called the Duffin Bed (Campbell, 1946) composed almost wholly of weathered Boyle clasts in a matrix of dolomitic mud almost certainly weathered and reworked from the Boyle (Ettensohn and others, 1988). In places, such as at the first described locality, the unconformity is a subtle angular unconformity. It is on this unconformity in the Stanford area that the halloysite-bearing residuum developed (Rice, 1962; Keller and others, 1966; McGrain and Kendall, 1972).

The halloysite, however, was not always present along the unconformity. In fact, the presence of flame structures into the black shales, as well as geochemical arguments in following sections, which necessitate the presence of the black shale before halloysite formation, indicate that halloysite development was definitely post-black shale and perhaps much later. It is likely that a pre-halloysite residuum was present, apparently related to pre-New Albany weathering on structurally related topographic highs. The highly variable distribution of units below the Boyle and New Albany formations on different fault blocks, as well as the presence of local angular unconformities and increased erosion near existing faults, all suggest Middle Paleozoic movement (Figure 4) on basement structural precursors; some of the movements may have occurred as growth faulting. Although evidence for both pre-Boyle and post-Boyle phases of movement is present (Figure 4), only the post-Boyle-pre-New Albany phase of structural movement was important in the formation of the residuum. Based on the local presence of relict chert nodules and silty black-shale partings at the main locality, the residuum apparently resulted from deep weathering of the cherty Boyle dolostone on the uplifted part of a fault block (Figure 4), although weathering of the Brassfield may have produced the residuum in the third exposure. That this kind of post-Boyle weathering and erosion did in fact occur is indicated by the presence of the Duffin breccias in the basal New Albany Shale. Erosion before or during the New Albany transgression

removed most of the residuum from the higher parts of the fault block, but the halloysite-bearing residuum reported in this study was preserved in erosional lows on underlying units. Whether or not the Boyle residuum was a paleosol is uncertain and probably not significant. The important fact is that the Boyle had undergone major weathering and erosion prior to New Albany deposition.

METHODS

Outcrop Description and Sampling Procedure

Based on the wet Munsell color value and lithology of the rocks, the outcrop was divided into ten zones (Figure 5). These zones are briefly described in Table 1, and the sequence of lithologic units is shown in Figure 2. Samples were

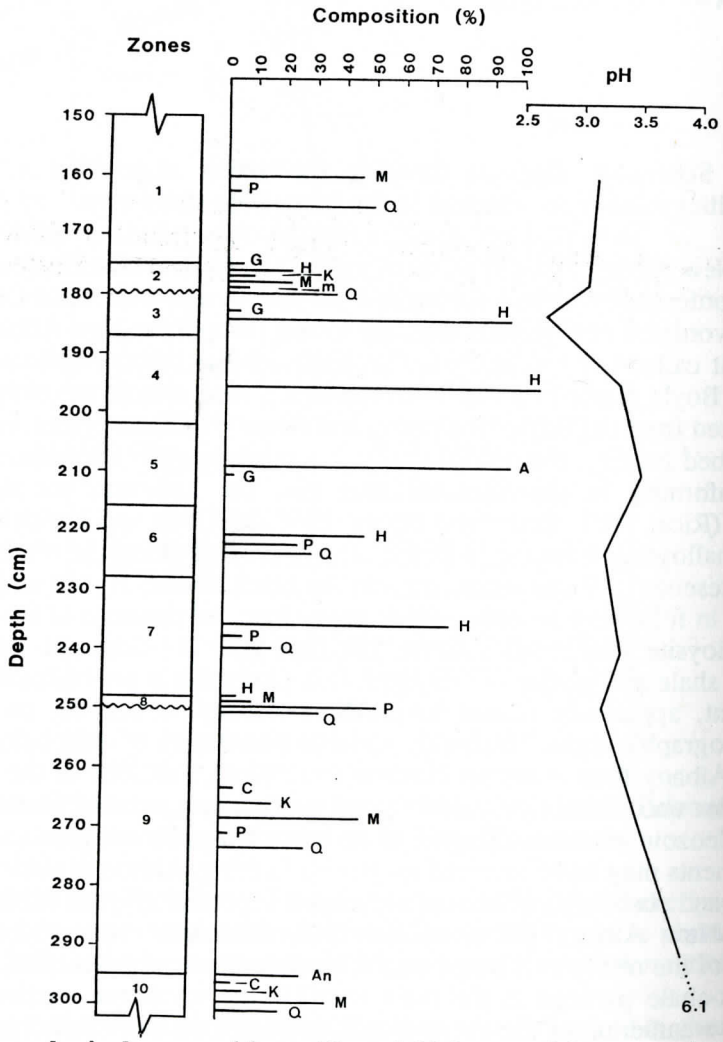

Figure 5. Mineralogical composition, pH, and thickness of the recognized zones in the exposure. Irregular lines represent stratigraphic unconformities. Abbreviations: H (halloysite); M ("Illite"); P (pyrite); Q (quartz); G (goethite); K (kaolinite); M (microcline); A (allophane); C (chlorite); and An (ankerite).

Table 1. Description of the section studied.

Zone	Munsell color value	approximate thickness (cm)	description
1	brownish black 5YR3/1	180	New Albany Shale, pyritic (Devonian).
2	brownish black 5YR3/1	10	New Albany Shale, lag zone with pyroclasts (Devonian).
3	reddish yellow 7.5 YR6/6	7	goethite-rich halloysite.
4	light gray 7.5YR8/1	15	halloysite.
5	yellowish brown 7.5YR8/l	14	goethite-rich allophane.
6	dark bluish gray I0GY4/1	12	organic-rich pyritic clay with euhedral quartz.
7	greenish gray 10GY3/1	20	abundant mottles and bands of halloysite.
8	dark greenish gray 10GY3/1	2	organic-rich, sandy pyritic clay.
9	bluish gray 10BG5/1	45	weathered, plastic Preachersville Shale (Ordovician).
10	bluish gray 10BG6/1	>500	relatively unweathered Preachersville Shale (Ordovician).

collected after removing approximately 20 cm of the outermost portion of the exposed beds. The samples were then wet-crushed or ground to pass through a 2-mm sieve and stored after air drying.

Because the halloysite developed on a Boyle residuum, some recent Boyle residua were collected from nearby localities and analyzed for possible comparison. Non-Boyle (Ordovician, sub- Chattanooga residua from central Tennessee; see Milton and others, 1955 and Conant and Swanson, 1961) were also collected and analyzed for comparison.

pH Measurements

Duplicate 10-g portions of the ground samples were suspended in 20 ml of deionized water. After initial stirring, the samples were allowed to sit for 60 minutes to attain equilibrium. The pH values were then obtained with a Corning pH meter furnished with an Orion KCl gel-filled calomel electrode and a glass electrode. Figure 5 shows the variations in pH from zone to zone.

Infrared spectrophotometry

One gram of oven-dried infrared quality KBr was mixed with 5-mg portions of the air-dried and heat-treated (110 °C for 24 hrs) halloysite or allophane

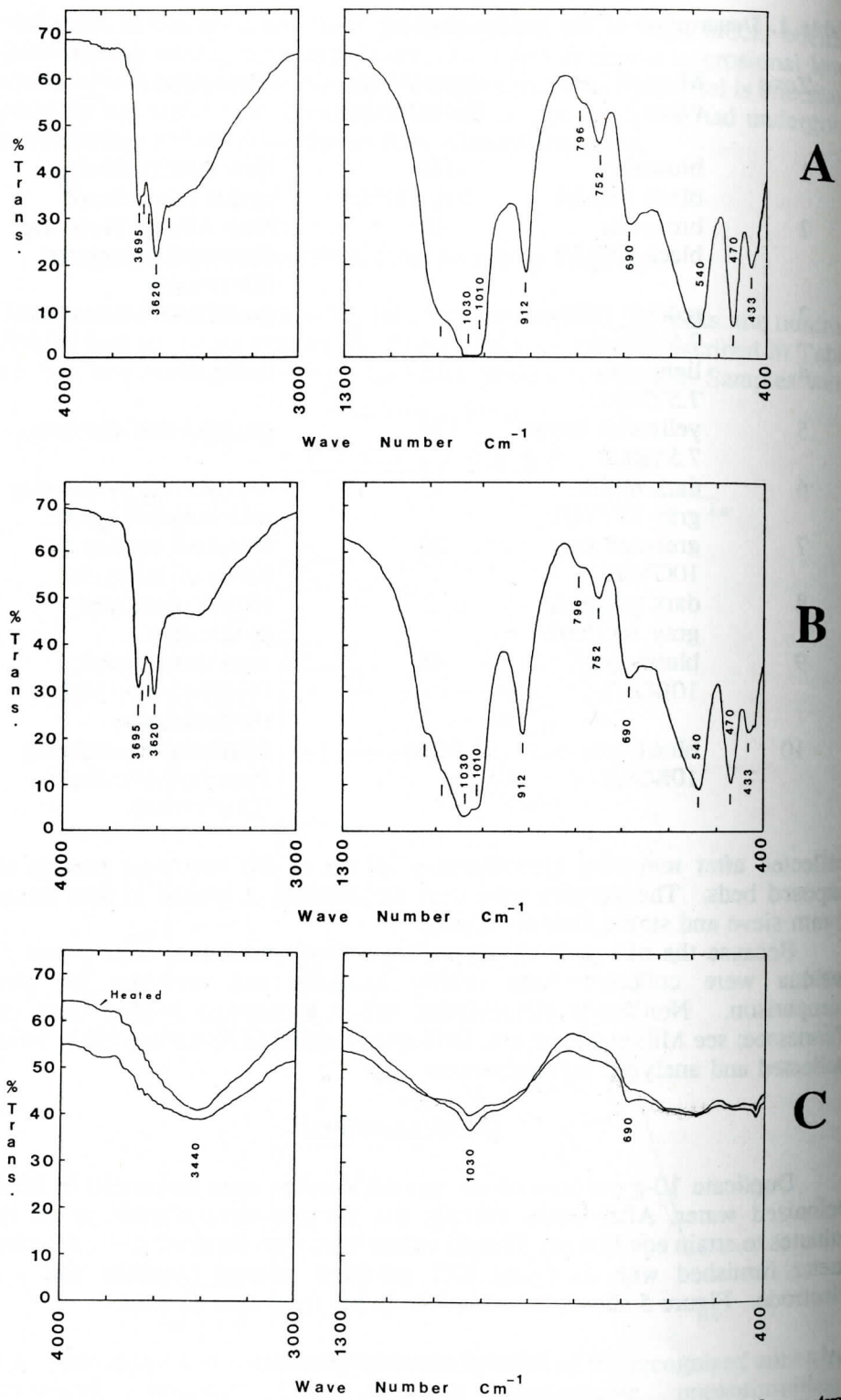

Figure 6. (a): Infrared spectra of hydrated Stanford halloysite. (b): Infrared spectra of heat-treated Stanford halloysite. (c): Infrared spectra of the Stanford allophane.

samples. This mixture was combined with ethyl alcohol and gently ground for two minutes with an agate mortar and pestle while the mixture dried. After the alcohol evaporated, the KBr-clay mixture was dried in a desiccator at room temperature. One hundred milligrams of this mixture was used to prepare the 1.3-cm pellets. Halloysite and allophane samples were scanned from 4000 to 200 cm -1 on a Perkin-Elmer Model 283 infrared spectrophotometer. Infrared absorption spectra of the halloysite and allophane beds in the regions 4000-3000 cm -1 and 13000-400 cm -1 are shown in Figure 6. The assignment of absorption bands was made through reference to the studies of Chukhrov and Zvyagin (1966) and van der Marel and Beutelspacher (1976).

X-ray methods

The 2-0.2 mm and <0.2 mm clay fractions were separated for X-ray diffraction analysis. Oriented clay specimens were prepared on a "Millipore" suction filter. Fifty milliliters of 1N MgCl and/or 30 percent glycerol in water

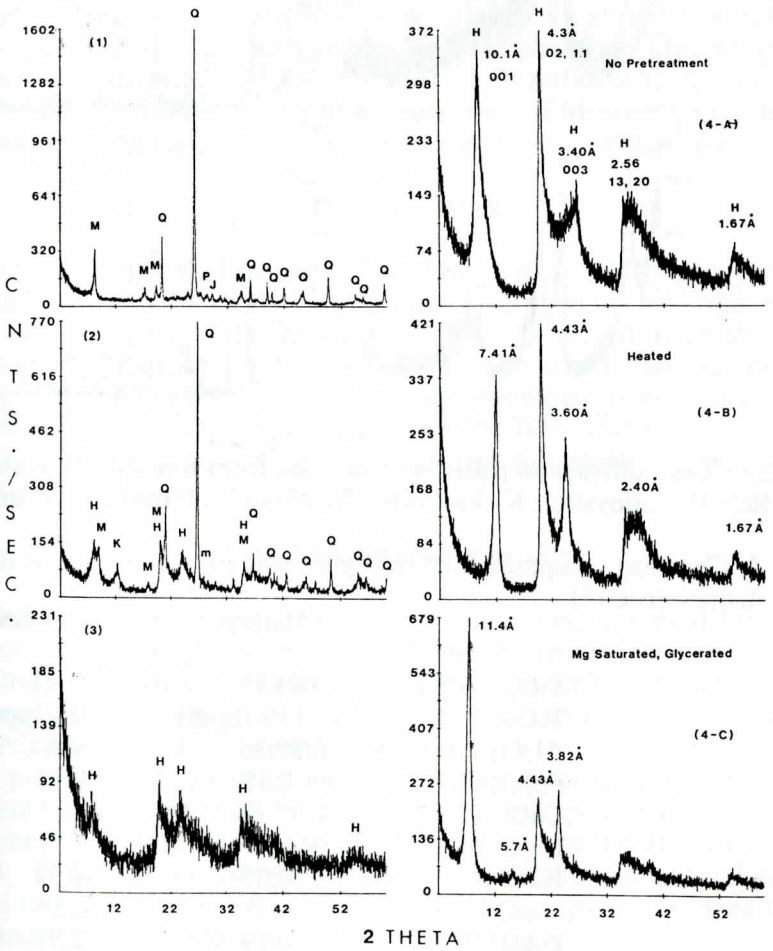

Figure 7. X-ray diffraction patterns of samples from zones 1-4. Abbreviations: H (halloysite); J (jarosite); K (kaolinite); M (muscovite and "illite"); m (microcline); P (pyrite); Q (quartz).

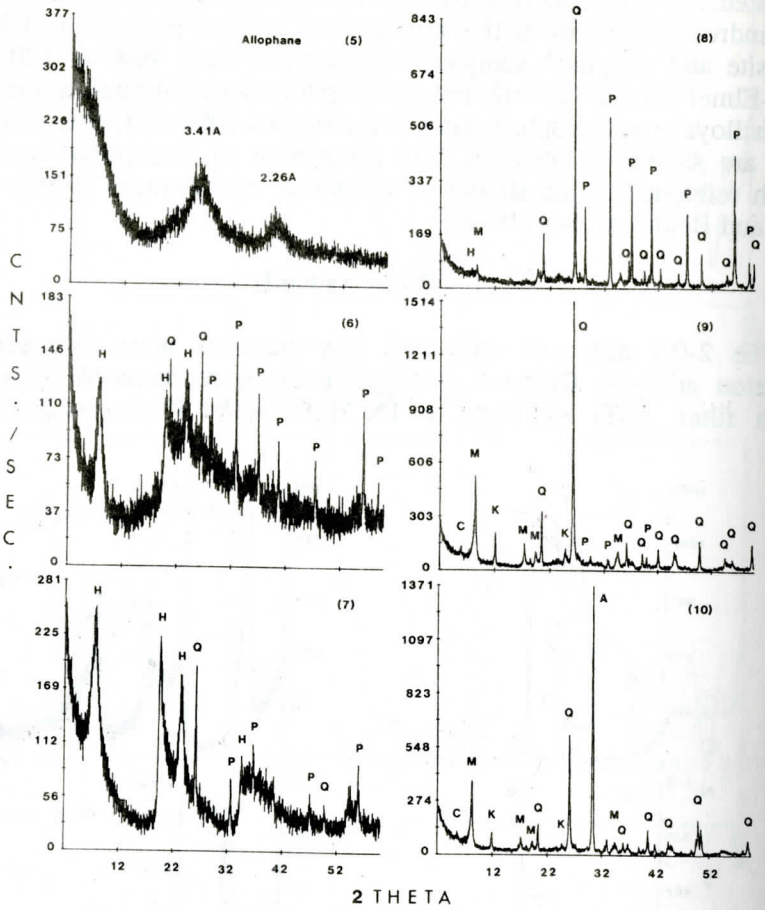

Figure 8. X-ray diffraction patterns of samples from zones 5-10. Abbreviations: C (chlorite); H (halloysite); K (kaolinite); M ("illite"); P (pyrite); Q (quartz).

Table 2. Chemical composition of halloysite and allophane beds as determined by x-ray fluorescence (*).

	Halloysite	Allophane
SiO_2	43.93	32.21
TiO_2	119 (ppm)	324 (ppm)
Al_2O_3	39.36	34.84
Fe_2O_3	0.15	1.61
CaO	0	0
MgO	0	0
K2O	0.05	0.12
Na_2O	0	0.05
P_2O_5	0.19	2.79
H_2O (+)** 14.00	27.40	
Total	97.69	99.16

* Percent by weight of the oven-dried material.
**Determined by TGA.

were passed through the samples. The clay layer on the filter was then inverted onto a glass slide. The samples were then scanned at 2° 2θ to 60° 2θ with a diffractometer using Ni-filtered Cu-Kα radiation. The XRD patterns of different zones are shown in Figures 7 and 8. Semi-quantitative mineralogy of the samples was determined using the peak heights of phyllosilicates (001), quartz (100), microcline (hkl), and pyrite (111). Figure 5 shows the variation in the mineralogy from zone to zone.

Three-gram pellets of randomly NH_4-saturated, ground and oven-dried (100° C) duplicates of the halloysite and allophane samples were prepared and analyzed for major elements on an automatic sequential wavelength dispersive XRF spectrometer. The resulting major elemental composition of halloysite and allophane beds is shown in Table 2.

Photomicroscopy

Samples of consolidated units were thin-sectioned and photographed; the most useful of sections came from the base of the black shale (zone 2; Figures 9C and 9D). Clean, fresh surfaces of air-dried samples from unconsolidated units were sputter-coated with gold and examined at magnifications as high as 26000X using a JOEL 25 scanning-electron microscope. SEM photomicrographs of the halloysite- and allophane-bearing residuum are shown in Figure 10.

Thermal studies

Magnesium-saturated samples of the halloysite and allophane were prepared for thermal gravimetric analysis (TGA) and differential scanning calorimetry (DSC). Five to 10 mg of the air-dried samples were placed in a platinum sample boat inside a quartz tube for TGA and DSC. The quartz tube was evacuated to 0.1 atm., and the furnace surrounding the tube was heated at a constant rate of 20° C/min from room temperature to 1000° C for the TGA, and at 10° C/min to 600° C for DSC analysis. The DSC and TGA patterns for samples from zones 4 and 5 are shown in Figures 11 and 12.

^{57}Fe Mössbauer spectroscopy

Pulverized samples from the different zones were prepared for Mössbauer spectroscopy without diluent and were held in the spectrometer pressed between plastic disks. Mössbauer spectra of samples from each zone were obtained at room temperature with a conventional constant-acceleration spectrometer using a ^{57}Co (Pd) source. The experimental spectra were computer fitted with an iterative program that calculated the best parameters for the different iron-bearing components in the spectrum by a X^2-minimization procedure. The Mössbauer spectra for different zones are shown in Figure 13 and the data are tabulated in Table 3. The presence of pyrite, goethite, jarosite, and szomolnokite were indicated in various zones by Mössbauer spectra. The goethite content of samples was estimated from its Mössbauer spectral intensity.

RESULTS AND INTERPRETATIONS

The prominence of mineralogic zonation in the halloysite-bearing interval

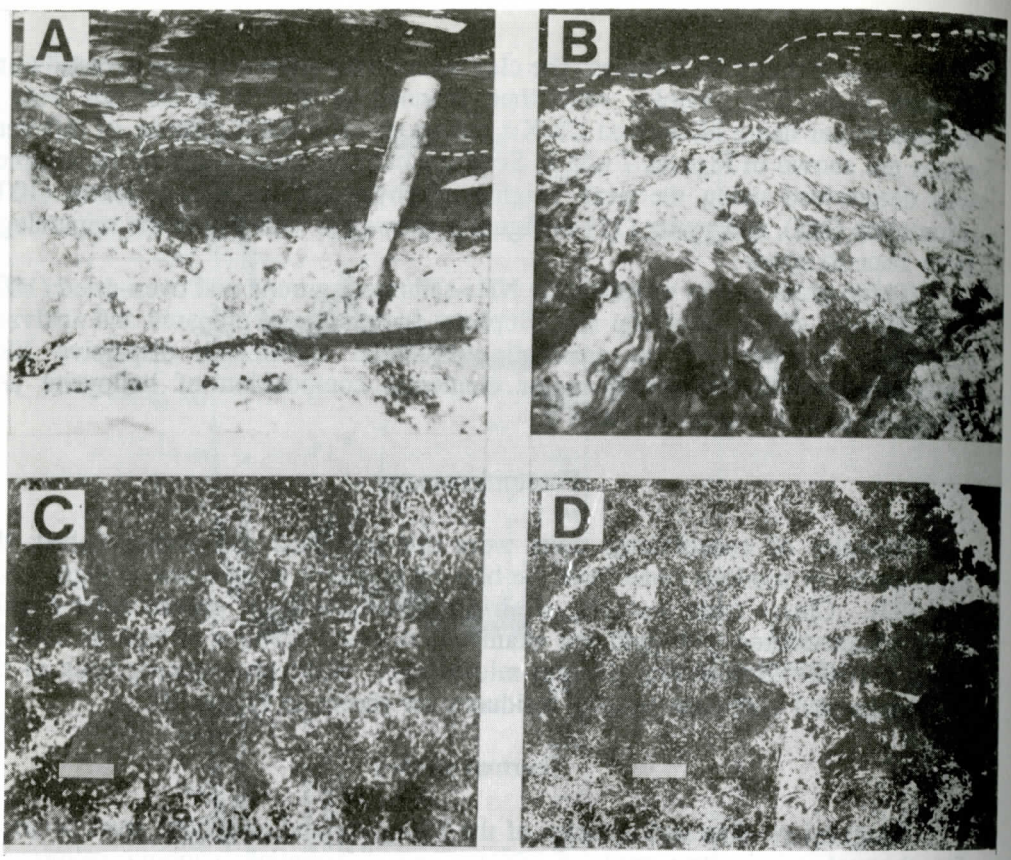

Figure 9. Photographs (A and B) of the halloysite-bearing residuum (dashed line separates the goethite-rich halloysite bed, zone 3, from the overlying lag, zone 2, and photomicrographs (C and D, bar=50 mm) of thin-sections from the lag (zone 2). A, halloysite below dashed line, black shales above; the white earthy material at base of photo is nearly pure halloysite of zone 4; note two-pronged halloysite flame structure into black shale at left center. B, black shales above dashed line, contortion of zones 3, 4, 5, and 6 below. C, curved, spicule-like shards in a pyroclast, now replaced by quartz; viewed in plane light. D, right-angle fracture filled with halloysite from below, cutting a silicified pyroclast.

suggests that much of the zonation may have been produced by the same processes that formed the halloysite and allophane. Inasmuch as the zonation is vertical, it is likely that most of the zones were produced by the downward migration of fluids, and that overlying zones influenced subjacent zones. Hence, it becomes important to understand the origin of each zone and how the alteration of any one zone influenced others, especially those below. Although the ten-zone sequence must now be viewed as a single entity to understand the origin of the halloysite, some of the zones originally had separate and distinct origins, for example, sedimentologic, pedologic, or diagenetic. In the following sections, we have used field evidence and data collected from the described lab procedures to develop inferences on the origin of each zone, their interrelationships, and their respective influence on the halloysite and allophane formation.

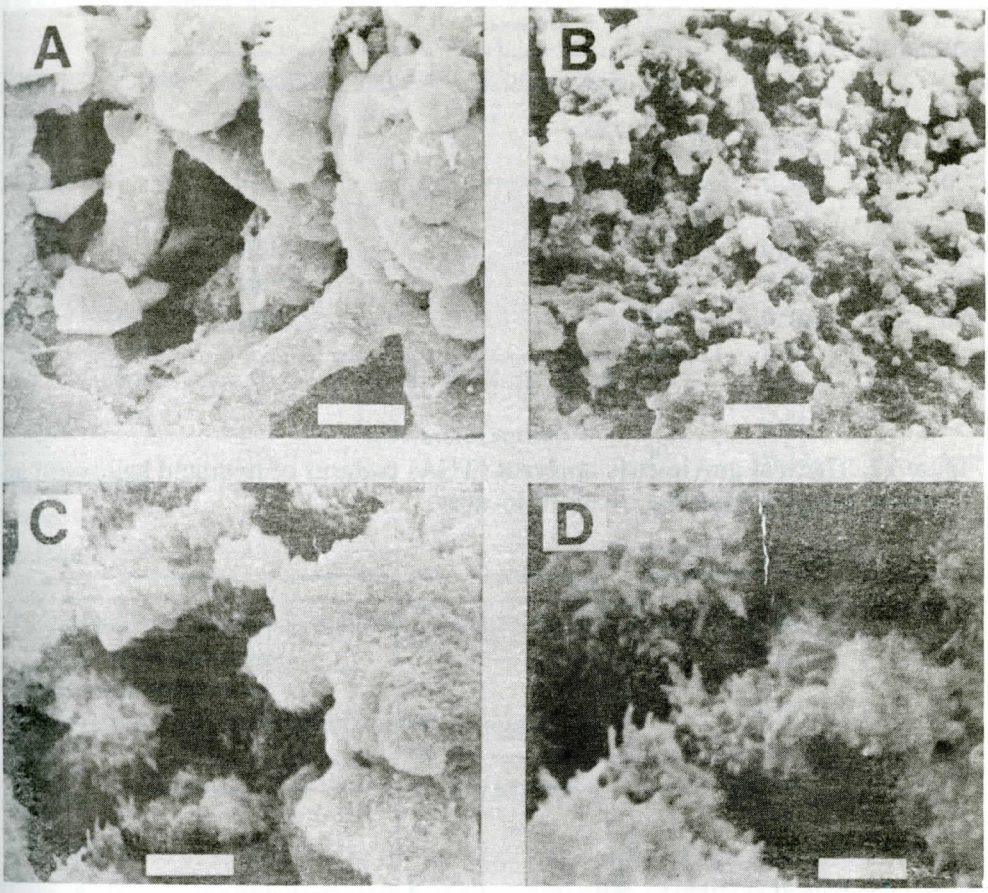

Figure 10. Scanning electron photomicrographs of allophane (A, bar=2 mm), and halloysite (B, bar=10 mm; C, bar=2 mm; and D, bar=1 mm) from the Stanford locality.

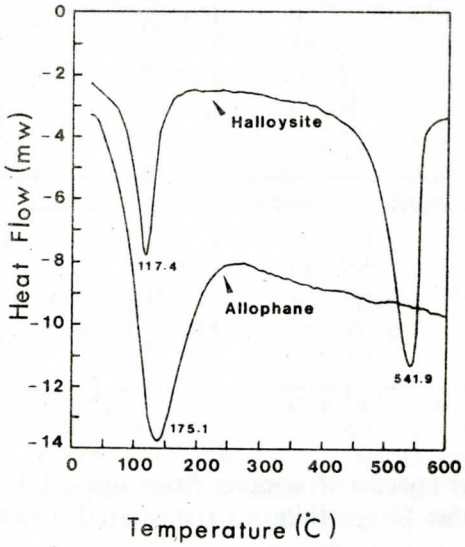

Figure 11. The differential scanning calorimetry (DSC) patterns of hydrated halloysite and allophane samples from the Stanford locality.

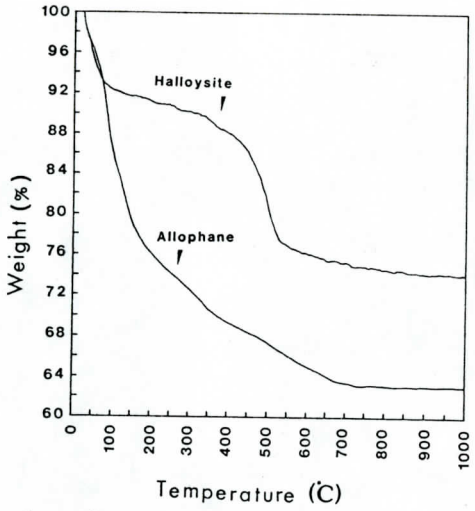

Figure 12. Thermal gravimetric analyses (TGA) patterns of hydrated halloysite and allophane samples from the Stanford locality.

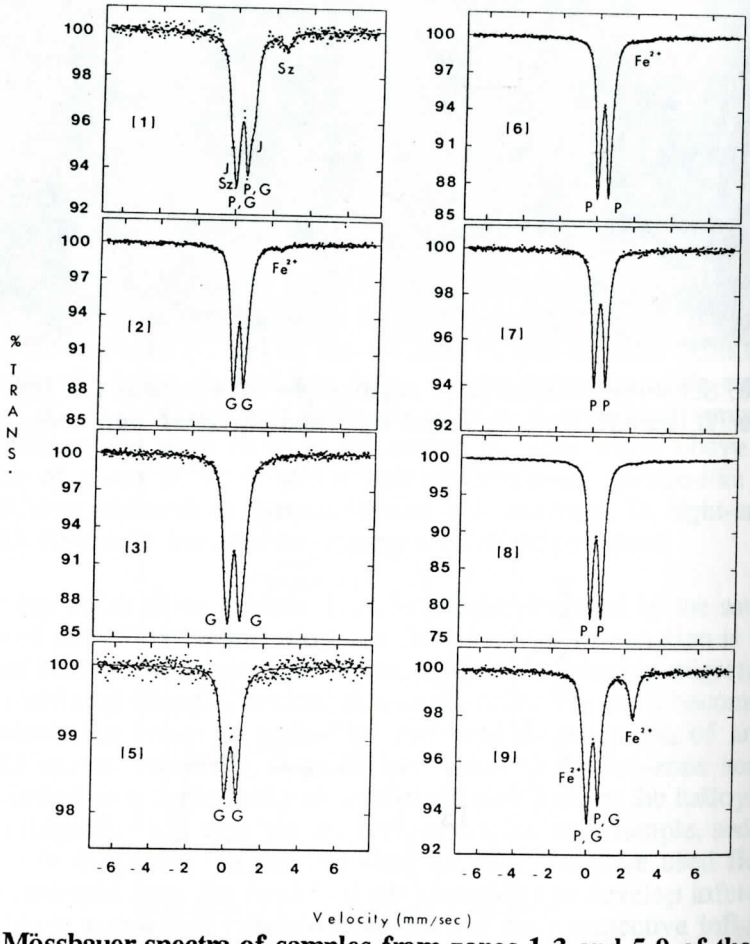

Figure 13. Mössbauer spectra of samples from zones 1-3 and 5-9 of the Stanford locality. Abbreviations: G (goethite); J (jarosite); P (pyrite); Sz (szomolnokite).

Table 3. Mossbauer data for the different zones.

	%Fe in					IS, QS (Pyrite/Goethite)*	
Zone	Pyrite	Goethite	Jarosite	Szomolnokite	Clay	IS	QS
1		66†	22	12	-	0.35	0.75
						0.36	0.53
2	-	97	-	-	3	0.36	0.53
						0.37	0.58
3	-	100	-	-	-	0.37	1.04
4		100**	-	-	-	0.35	0.60
5	-	100	-	-	-	0.36	0.64
6	>99	-	-	-	<1	0.31	0.60
7	100	-	-	-	-	0.31	0.60
8	100	-	-	-	-	0.31	0.61
9		70†	-	-	30	0.33	0.58
Standard values							
Pyrite						0.31	0.61
Goethite					0.37	0.55-0.75	

* Isomer shift and quadrupole splitting parameters for main iron-bearing absorption (pyrite/goethite).

** Very weak absorption.

† Parameters indicate possible mixture of pyrite/goethite.

Zone 1

This zone consists wholly of the Upper Devonian (Famennian) New Albany Shale, a pyritic, organic-rich, black shale, which has experienced almost none of the alteration characterizing the underlying zones. Although this zone is wholly the product of sedimentological processes, it is nonetheless extremely important, because pyrite in the zone is the principal source of downward-moving sulfuric acid which is necessary for the dissolution of the Al- and Si-bearing minerals and consequent halloysite formation. Figures 5 and 7 (zone 1) show that "illite", quartz, and pyrite are the major inorganic constituents in this zone. It appears to us that oxidation of the pyrite generated sulfuric acid (see Vuorinen and others, 1983) which resulted in alternation of the original sediments and generated a relict pH of 3.1 in our analysis (Figure 5), although Keller and others (1966) reported that undiluted seep-waters from this zone may have pH values below one. The acid generated in this zone is capable of gradually dissolving the octahedral and tetrahedral sheets of "illite", releasing potassium ions and Al- and Si-oxyhydroxides which are carried downward with percolating waters. As this water moves downward, continuing inorganic oxidation of pyrite further reduces the pH (Figure 5).

The jarosite, goethite, and szomolnokite noted on the Mössbauer spectra of samples from this zone (Figure 13), as well as the yellow, X-ray-amorphous ferric hydroxides colloquially known as "yellow boy" found on the exposure, are byproducts of pyrite oxidation, and sulfuric acid formation may appreciably retard the further oxidation of ferrous iron (Singer and Stumm, 1970). However, in the presence of acidophilic, iron-oxidizing thiobacilli, this oxidation rate can be

accelerated five to six orders of magnitude (Nordstrom, 1982). In the resulting conditions of low pH and high sulfate concentration, jarosite commonly forms, whereas goethite results from the hydrolysis of ferric iron to ferrihydrite and its subsequent dehydration. Szomolnokite, a readily soluble hydrated iron sulfate, on the other hand, is a product of pyrite oxidation in drier environments (Nordstrom, 1982). However, in conditions resulting from the dilution of percolating acidic solutions by fresh meteoric waters, "yellow boy" will precipitate (Stumm and Morgen, 1981; Brady and others, 1986).

The formation of the above iron compounds is clearly secondary to pyrite oxidation. Nonetheless, these compounds are important because their formation may mediate or buffer later stages of acid formation.

Zone 2

The zone is the basal lag horizon or "bone bed" that everywhere defines the base of the New Albany Shale. This 2-cm thick horizon is a sedimentological zone produced by reworking and condensation over a relatively long period of time (Middle Devonian to early Late Devonian: Givetian-Frasnian) with little sedimentation. The deposit is coarse-grained, permeable, goethite-stained and commonly contains phosphate nodules. Air-fall tuffs are not uncommon in these lags, and the tuffaceous nature of this deposit is evident from thin-sections showing lithic tuffs with devitrified glass shards in altered pyroclasts (Figure 9C) and horizons of crystal tuffs composed almost entirely of euhedral feldspar crystals, now altered or dissolved away. Thin-section examination also revealed glauconite, quartz sand, pyritized spores, vermicular kaolinite, as well as phosphate nodules and bone fragments composed of collophane. Halloysite-filled fractures of all sizes were observed penetrating this lag zone and lower parts of the overlying New Albany Shale (Figures 2 and 9A). Many of these filled fractures have the appearance of flame structures (Figure 9A) suggesting the upward movement of halloysite or pre-halloysite residuum during compaction or soft-sediment deformation. Basal parts of the lag have also been altered to halloysite.

The association of the lag zone with the underlying halloysite may be fortuitous in this case, but in some areas like Japan and New Zealand, the alteration of volcanic ash beds has generated halloysite-rich soils (Wada, 1977; Kirkman, 1981). Although there is no evidence that any of the volcanic ash in the lag zone has been altered to halloysite, it is possible that the concentration and downward movement of aluminum- and silicon-oxyhydroxides leached from the ash may have facilitated halloysite formation. Moreover, vermicular kaolinite, like that seen in thin sections, is commonly reported from volcanic ash partings in coal beds (Williamson, 1970; Addison and others, 1983). It is likely that this kaolinite and the sparse szomolnokite seen in this zone (Figures 7 and 13) formed during drier periods when the rapid percolation of descending waters temporarily ceased (Chukhrov and Zvyagin, 1966; Nordstrom, 1982).

The abundance of goethite over iron sulfates in this zone (Figure 13) probably reflects the porous nature of the lag. Inasmuch as sulfate anions will successfully compete with hydroxyls to prevent the crystallization of goethite, the presence of goethite probably indicates that most sulfate anions were flushed out of this permeable zone.

Zone 3

This is a diagenetic zone which includes the uppermost two to twelve centimeters of reddish-yellow-colored halloysite and goethite (Figures 2, 9A, and 9B), which presumably defines the top of the former Boyle residuum. X-ray diffraction (Figure 7) and Mössbauer spectra (Figure 13) show that halloysite and goethite are the major constituents. The abundance of goethite is responsible for the intense light brown color. However, the cementing property of goethite, which diminishes the parallel stacking propensity of phyllosilicates, and the fluorescence of iron in Cu K radiation, apparently reduced the intensity of diffracted XRD peaks for halloysite (Figure 7).

Although most of the goethite in this zone was probably derived from oxidation of pyrite in the overlying lag zone, Keller and others (1966) showed that appreciable amounts of sulfate anions are largely absent from the zone. This absence is important because it may have facilitated the formation of goethite for reasons noted in the discussion of zone 2 above (Brady and others, 1986). In the absence of jarosite and ferrihydrite, which would have had a buffering effect (Miller, 1979, in Goldhaber and Kaplan, 1982), the pH dropped to values as low as 2.7 in our determinations, and seep waters are probably more acidic. At these pH values, goethite is soluble and would have moved downward freely to stain the halloysite.

Zone 4

The next 20 to 40 cm is the major, diagenetic halloysite-bearing zone; it consists largely of light gray (7.5YR8/1) halloysite with locally occurring, irregularly shaped bodies of porcelaneous halloysite up to 10 cm wide.

The most diagnostic characteristic for halloysite is the change in the basal spacing (Carr and Chih, 1971) from 10.1 A in the air-dried sample to 7.4 A on heating to 110° C for 24 hours and its subsequent expansion to 11.4 A upon glyceration (Figure 7,4-A through 4-C). No 7 A halloysite was detected. The DSC pattern for samples in zone 4 (Figure 11) shows two endothermic peaks at 117 and 541° C, which are also typical of halloysite (Holdrige and Vaughan, 1957). The TGA pattern (Figure 12) shows two main regions of weight loss which results in a 28-percent weight reduction at 1000° C. Figures 10C and 10D show the typical tubular nature of halloysite; Figure 10B shows that zone 4 is porous with pores up to 5 mm in diameter.

The chemical analysis (Table 2) shows that SiO_2, Al_2O_3 and water are the major chemical constituents, though titanium, phosphorus, potassium, and iron also are present. The titanium probably originated in the overlying zones through dissolution of octahedral sheets in mica and was transported to this zone as TiO_2 and $Ti(OH)_4$ (Weaver, 1976). At pH values above 2.5, TiO_2 precipitates, explaining its presence in the halloysite. $Ti(OH)_4$, however, stays in solution and will continue to move downward until slightly higher pH levels are encountered. These hydrous oxide gels of Ti then precipitate and with time convert to granular aggregates of small anatase crystals. These crystals are then attracted to each other and to kandite layers by electrostatic and/or chemical bonding (Weaver, 1976). Most of the phosphorus, on the other hand, is apparently related to dissolution of collophane in zone 2 and is probably adsorbed onto the positively

charged edges of kandite layers as phosphate anions (van Olphen, 1977). The potassium was probably derived from the dissolution of clays and feldspars in zones 1 and 2, and with the sulfate flushed from overlying zones, has formed the mineral alunite, which was observed in thin section with the halloysite. The Mössbauer spectrum of this zone showed a very weak, broadened absorption that appears to correspond to goethite, but it may have arisen from another phase, such as the Fe^3+ in alunite.

The ratio of the intensity of the IR absorption peak at 3695 cm^{-1} (surface OH groups) to that at 3620 cm^{-1} (octahedral OH pointing to the empty inner lobes) was suggested by Chukhrov and Zvyagin (1966) to be an empirical indicator of the degree of structural perfection. Moreover, Nagasawa and Miyazaki (1976) used the A_{3470}/A_{3620} ratio of hydrated and dehydrated halloysite for "age" (degree-of-order) determinations in samples collected from different parts of Japan. The older the halloysite, the lower the intensity of its inner Al-OH stretching vibration and the higher the A_{3670}/A_{3620} ratio. Older halloysites, therefore, lose their interlayer water more easily (Nagasawa and Miyazaki, 1975). Our determination of this ratio for the Stanford halloysite showed an increase from 0.83 to 0.96 upon heating, indicating that greater order resulted as most of the interlayer water was driven off (Figure 6A-B) and suggesting an "old age" in their classification.

The DSC patterns (Figure 11) show that the Stanford halloysite begins losing its interlayer water at temperatures just above 25° C. However, most of the interlayer water was lost at about 117° C. Between 117° C and 400° C, an additional four-percent weight loss was observed (Figure 12), which is probably due to the escape of water persisting as islets. At 400° C, however, the kandite layers begin to undergo dehydroxylation (Figure 11), which peaks at 542° C. Between this temperature and 800° C, another three-percent weight loss was observed, probably due to dehydroxylation of inner particulate octahedra.

The above characteristics clearly indicate the identity of the halloysite, but the exact origin of the halloysite is not as certain. We postulate that two factors were especially important for the formational processes. First was the nature of the Boyle residuum. The Boyle had already probably been weathered prior to burial by the black shales so that if the resulting residuum was similar to modern residua developed on the Boyle, all the carbonate had been leached, the dominant illitic clay had been altered to a hydroxy-Al-interlayered vermiculite or vermiculite, and silica derived from residual chert would have been present in high concentrations. Leaching of the carbonate and other weathering processes no doubt increased the porosity and permeability of the residuum, thereby providing greater access for downward percolating solutions. The formation of vermiculite greatly increased the amount of surface area available for reaction, and would have thereby accelerated the dissolution of clays by acid solutions.

The abundance of silica in the residuum relates to the second factor, namely the molar ratio of Si to Al. Keller and others (1966) measured the concentrations of Si and Al in seep waters from the New Albany Shale (zone 1) and from the halloysite (Zone 4). They found that the Si concentrations decreased from 78 ppm in Zone 1 to 16.2 ppm in zone 4. Aluminum concentration decreased from 68 ppm in zone 1 to 38 ppm in zone 4. In other words, the H_2SiO_4 concentrations at the top of halloysite bed attain values near saturation. At the bottom of the halloysite bed, however, the silica content of the seeping waters is dramatically decreased. Although, both sets of concentrations for Si and Al fall within the stability field of halloysite (Hem and others, 1973), comparison of the molar ratios of Si/A1 in these

two zones is revealing. In zone 1 this ratio reaches a value of 1.23, which exceeds the theoretical value for halloysite. In zone 4, the ratio decreases to 0.57. Comparison of the molar ratios suggests that the percolating waters were progressively depleted in Si as they passed through zone 2, and that molar ratios higher than 0.57 of Si to Al are prerequisite for halloysite formation. Even though dissolution of clays and residual chert in the residuum provided substantial silica, it evidently was not sufficient to elevate the ratio to the point of halloysite formation. Only with the addition of silica dissolved from the overlying shales and tuffaceous lag zone (zone 2) was the equilibrium constant exceeded in favor of halloysite precipitation. Under the given chemical and moisture conditions, halloysite seems to have formed more rapidly than the thermodynamically more stable 1:1 phyllosilicate, kaolinite.

If the above scenario is correct and a higher Si/A1 ratio is the critical factor, then halloysite formation should be expanding upward. This speculation is supported by our previous observation that basal parts of the lag zone, which were never part of the Boyle residuum, are indeed being altered to halloysite.

Zone 5

In much of the section, an irregular yellowish-brown (7.5YR4/6) zone, 10 to 20 cm thick, underlies zone 4. This is a diagenetic zone wholly within the residuum; a combination of x-ray diffraction (Figure 8, no.5), DSC and TGA analyses (Figures 11 and 12), Mössbauer spectroscopy (Figure 13, no.5), infrared spectrophotometry (Figure 6C), and SEM photomicrography (Figure 10A) indicates that it is composed almost entirely of goethite-rich allophane (Figure 5).

The x-ray diffraction pattern (Figure 8, no.5) is typical of non-crystalline materials with little internal three-dimensional atomic order (Okada and others, 1975). Moreover, relatively pure samples from this zone show a DSC endothermic peak at 175° C (Figure 11) and a nearly 28-percent weight loss between 25° C and 200° C during TGA analysis; at 1000° C, a 36-percent weight loss was apparent in TGA (Figure 12). These results are typical of allophane (Wada, 1977).

The chemical analysis (Table 2) of this allophane indicates an Al_2O_3:SiO_2 molar ratio of 1:1.6. With a ratio of this magnitude, it is possible that some of the tetrahedral sites are occupied by aluminum (Henmi and Wada, 1976). Nonetheless, at the relatively low pH values encountered in this zone (Figure 8), the oxyhydroxides of Al and Fe are positively charged, and most of the phosphorus (Table 2) is probably nonspecifically adsorbed by Al(OH) and Fe(OH) groups (Wada, 1977; Parfitt and others, 1980). The TiO_2 (Table 2) is probably present under the same conditions as described for the halloysite zone, and Mössbauer spectra (Figure 13, no.5) indicate that all the iron is present as goethite.

Finally, infrared spectrophotometry showed that the IR absorption band at 1035 cm^{-1} increased upon the heating of this allophane to 110° C (Figure 6C). This increase is probably related to the composition of the outer surfaces of the allophane particulates (Parfitt and others, 1980; van der Gast and others, 1984).

The "micro-columnar" nature of this allophane (Figure 9A) suggests that it formed through precipitation as Al- and Si-rich solutions passed through the zone. No imogolite or other intermediate phases between allophane and halloysite could be detected.

Whether or not halloysite or allophane is precipitated seems to be related to

the Si concentration of the seeping waters. Halloysite precipitation, however, must have effectively depleted much of the silica from solution, thereby lowering the Si concentration to the point that its formation ceased and allophane precipitation began. Again, the threshold level at which allophane precipitation occurred, is not known, but where it was attained, halloysite abruptly gives way to allophane and zone 5 begins. Locally within the allophane, pods of halloysite are still present, but these are localized around relict chert nodules from the Boyle. In these cases, the presence of excess silica from the chert apparently increased the Si concentration to the point that halloysite could again be precipitated.

Zone 6

The dark bluish-gray (I0BG4/1), organic-rich clays of this zone differ markedly from overlying zones, but they are nonetheless an integral part of the zonal sequence and compose a diagenetic zone within the residuum; the zone is commonly 10 to 15 cm thick.

The major difference between this zone and those above is the presence of organic matter, pyrite, and euhedral quartz. The organic matter is mostly alkaline-insoluble and either originated in place or was derived from the overlying black shales or overlying parts of the Boyle residuum. We believe that the organic matter remains in a reduced state because it was deposited or persisted in place below the water table. If this is the case, then the top of zone 6 marks the position of a paleo-water table. Because any drainage is extremely slow at the water table, oxygen is not replaced rapidly so that rapid bacterial consumption of oxygen may have lowered the Eh, resulting in biological reduction of iron sulfates to pyrite (Doner and Lynn, 1977).

The origin of the euhedral quartz is similarly related to the former presence of a water table. Excess silica no doubt also moved downward to the level of the water table where sluggish waters at the top became supersaturated with respect silica. Supersaturation and the lowering of acidity through biological reduction of sulfates, apparently created the necessary conditions for the precipitation of quartz (Figure 8, no.6); some of the resulting euhedral quartz crystals have attained the size of coarse sand.

All of the above processes would have continued as the water table migrated up or down in section, with the result that organic matter, pyrite, and euhedral quartz are distributed throughout the zone.

Halloysite is also present in the zone, but its presence is apparently related to other factors which arose in the zone below when the water table dropped.

Zone 7

Except for the lighter greenish-gray color (I0GY6/1) and a greater abundance of halloysite (Figures 5 and 8, no.7), this zone is essentially a continuation of the zone above. It is a diagenetic zone, up to 20 cm thick, which occupies the remainder of the residual interval and is characterized by abundant mottles and bands of halloysite. Many of these bands have been intensely contorted (Figures 2 and 9B) due to compaction or soft-sediment deformation.

Keller and others (1966) demonstrated an increased silica content from interstitial solutions in this zone, and we believe that this is related to the increased presence of halloysite in the zone. We suggest that halloysite formation began as

drainage improved or as the water table dropped. With a dropping water table, the downward percolation of acid waters would have resumed, and the resulting acid dissolution of euhedral quartz would have provided enough excess silica to initiate halloysite precipitation again.

If the above model is correct, it means that "halloysitization" would have increased in intensity as the water table lowered. It also follows, that the amount of pyrite and euhedral quartz would have decreased as noted (Figure 5) due to oxidation and dissolution, respectively.

As to why halloysite formation was more effective in this zone than in zone 6 we are uncertain. However, the increase may be related to more rapid rates of water-table decline, or to an increased contribution of acid from oxidation of pyrite in the zone above, or perhaps more significantly, to increased porosity and permeability in the zone. Indeed, much of the halloysite banding and mottling follows coarser, more porous horizons; some of the banding may even reflect relict bedding.

Zone 8

A few centimeters of sandy, pyritic clay at the base of the Boyle residuum characterize zone 8. This zone was originally a sedimentologic condensation or lag zone which is common at the base of the Boyle Formation. Some of the micas and detrital quartz found in the zone probably reflect sedimentary reworking of underlying Ordovician rocks during the initial Boyle transgression. However, because of its position at the base of the residuum and atop the relatively impermeable, plastic clays of the underlying zone, zone 8 apparently served as a site of final accumulation for many downwardly moving materials such as organic matter, silica, iron and sulfate and for the products of resulting interactions. Hence, the zone has large concentrations of organic matter and pyrite and lesser amounts of euhedral quartz and halloysite (Figures 5 and 8).

The accumulation of some of these materials also may have been facilitated by an apparent stasis of the water table at this horizon.

Zone 9

This zone consists of 40 to 60 cm of weathered, bluish-gray (I0BG5/1) plastic clay. Although all the carbonate has been leached from the zone, the facts that the clays are relatively unweathered (Figure 7, no.9) and that the detrital quartz is still intact suggest that the zone has not been subjected to a great deal of pedogenic weathering nor to the effects of intense acidification like the zones above. This zone may represent the B-horizon of a relatively immature soil.

The Mössbauer spectra for the zone (Figure 13, no.9) show the presence of pyrite, goethite, and ferrous iron, which is probably associated with the chlorite structure and responsible for the asymmetry of component peaks. The goethite in the sample is probably a product of contamination or of recent formation along joints after the opening of the road cut.

Comparison of X-ray diffraction patterns from this zone (Figure 7, no.9) with those from the parent rock below (Figure 7, no. 10) shows an increase in kaolinite content. This kaolinite may have formed as the result of acid weathering in a poorly drained environment.

This zone and the underlying one were probably not a part of the zonal profile

developed as a result of the downward percolation of acid solutions from the New Albany. "Halloysitization" and intense acid dissolution apparently stopped at the Boyle lag horizon (zone 8). The cessation of these processes at the lag is probably related to the relatively impermeable nature of the plastic clays in the zone and to the fact that this and underlying lithologies were almost certainly within the saturated zone until very recently, perhaps as recently as the opening of the roadcut.

Zone 10

This zone is a relatively unweathered example of the Preachersville Shale Member of the Drakes Formation (Figures 2- 4). Only about 5 m is present in this exposure, but elsewhere in the area the unit attains thicknesses as great as 20 m (Shawe and Wigley, 1975). Dolostone and limestone beds are present in the unit explaining the high pH of the zone relative to those above (Figure 5). However, the dolostone sample analyzed proved to be ankeritic (Figure 8, no.10), indicating some replacement by iron, presumably derived from zones above.

Like the zone above, "halloysitization" and intense acid weathering apparently have had little effect here.

DISCUSSION and CONCLUSIONS

The prominence of the lithologic and mineralogic zonation in the halloysite-bearing rocks described herein suggests a set of geologic and chemical controls governing the formation of certain aluminosilicates which may be applicable elsewhere. This zonation is basically a product of the alteration, enrichment and depletion of various chemical and organic phases as meteoric water descended through a geologic section. However, not just any geologic section would have been adequate. The section must contain sources of acid, silica, and alumina and overlie a porous, permeable horizon above the water table. In the interval we have studied, the pyritic, tuffaceous New Albany Shale served as the source rock, and an underlying residuum provided the porous, permeable horizon for alteration. The occurrence of the section on a fault block in a fault zone that experienced periodic reactivation during and after the Paleozoic was apparently responsible for elevation above the water table and the later preservation of the deposit.

Although ten zones have been recognized, they can be consolidated into five process-related intervals of different origin: 1) an acid and silica source, 2) an interval of alteration and relative silica enrichment, 3) an interval of alteration and relative silica depletion, 4) an interval of alteration and accumulation above the water table and above a permeability barrier, and 5) an unaffected interval below the permeability barrier. The pyritic, tuffaceous rocks of the New Albany Shale (zones I and 2) were the sources of percolating silica- and alumina-rich acid solutions. The underlying halloysite-rich zones in the upper part of the residuum (zones 3 and 4) represent an interval of acid dissolution of clays and accompanying silica enrichment from above. Consumption of silica during halloysite formation generated an underlying interval of acid alteration, but with relative silica depletion. The result was a zone in the residuum (zone 5) composed almost entirely of allophane. The next three lower zones (zones 6, 7, and 8) largely represent an interval of accumulation at the base of the residuum. Because of an underlying permeability barrier and the presence of the water table, chemical and

organic phases, which were not consumed above, accumulated and interacted here. The fact that the accumulation occurred in alternating saturated and unsaturated conditions near the top of a fluctuating water table accounts for the variety of mineralogic and organic phases found in these zones. Finally, zones 9 and 10 form an interval largely unaffected by above processes because of their location within or below the permeability barrier.

The chemical and mineralogic analyses of the zones suggest a definite chemical and physical relationship between halloysite and allophane. Both halloysite and allophane seem to form in well-drained regimes, but halloysite precipitation is favored under conditions of higher Si/A1 molar ratios. Above a threshold value of this ratio, as yet undetermined, halloysite precipitation will be initiated. In the case of the Stanford halloysite, the excess silica needed to surpass that threshold boundary was apparently provided by the dissolution of clay and feldspar in the overlying New Albany Shale. However, localized occurrences of halloysite in other zones from the same exposure indicate that dissolution of chert nodules and epigenetic quartz may also provide the additional silica. Once the Si/A1 molar ratio declines below the threshold level, due to utilization of Si in halloysite precipitation, allophane apparently will be precipitated. This means that in supergene situations such as occur in this deposit, allophane should be expected immediately below the halloysite.

Clearly, this halloysite is the product of a larger interaction between structural, stratigraphic and hydrologic conditions, but the occurrence is not unique. Many of the so-called "fireclays" that are noted by drillers on the unconformity below the Devonian black shale in eastern Kentucky may represent similar halloysite deposits. Any situation where pyrite-rich sediments overlie residua on unconformities may provide the potential for halloysite formation.

ACKNOWLEDGMENTS

We wish to thank professors R.I. Barnhisel, J.D. Hem, and, W.D. Keller who critically read earlier versions of the manuscript. We wish to thank the following people who assisted with the various procedures and analyses: Dr. Frank Huggins for Mössbauer data, Mr. Terry Sobecki for TGA and DSC analyses, Mr. T.A. Moore for photography, and the Kentucky Energy Cabinet Laboratories for the XRF data. Parts of this research were supported by an NSF grant (EAR-85-113414) to the senior author.

REFERENCES

Addison, R., Harrison, R.K., Land, D.H., and Young, B.R.,1983, Volcanogenic tonsteins from Tertiary coal measures, East Kalimantan, Indonesia: Int. J. Coal Geol.,v.3, p.1-30.

Brady, K.S., Bigham, J.M., Jayres, W. F., and Logan, T.R.,1986, Influence of sulfate on Fe-oxide formation: comparisons with a stream receiving acid mine drainage: Clay & Clay Minerals, v.34,p. 266-277.

Callaghan, E.,1948, Endellite deposits in Gardner Mine Ridge, Lawrence County, Indiana: Indiana Dept. Conserv., Div. of Geology, Bull. No. 1, 47p.

Carr,R.M., and Chih, H.,1971, Complexes of halloysite with organic compounds: Clay Minerals, v.9, p.153-166.

Chukhrov, F.V., and Zvyagin, B.B.,1966, Halloysite, A crystallochemically and

mineralogically distinct species: Proc. Int. Clay Conf., Jerusalem, p.11-25.
Conant, L.C., and Swanson, V.E., 1961, Chattanooga Shale and related rocks of central Tennessee and nearby areas: U.S. Geol. Surv. Prof. Pap. 357, 91p.
Crawford, T.J., and McGrain P.,1963, Porcelaneous halloysite beneath New Albany Shale in Lincoln County, Kentucky: Geol. Soc. Am. Spec. Paper 76, p.241-242.
Dever, G.R., Jr., Hoge, H.P., Hester, N.C., and Ettensohn, F.R., 1977, Stratigraphic evidence for Late Paleozoic tectonism in northeastern Kentucky: Eastern A.A.P.G. 5th Ann. Mtg., Field Trip Guidebook, Kentucky Geol. Surv., 80p.
Doner, H.E., and Lynn, W.C. 1977, Carbonate, halide, sulfate, and sulfide minerals, *in* Minerals in Soil Environments (T.B. Dixon and others., eds.): Soil Sci. Soc. Amer.,p.75-98.
Ettensohn, F.R., Miller, M.H., Dillman, S.B., Elam, T.C., Geller, K.L., Swager, D.R., Markowitz, G., Woock, R.D., and Barron, L.S., 1988, Characterization and implications of the Devonian-Mississippian black-shale sequence, eastern and central Kentucky, U.S.A.: pycnoclines, transgression, regression, and tectonism, *in* Devonian of the World, Proceedings of the Second International Symposium on the Devonian System (N.J. McMillan, A.F. Embry, and D.J. Glass, eds.): Canadian Society of Petroleum Geologists Memoir 14, v.2, p.323-345.
Goldhaber, M.B., and Kaplan, I.R., 1982, Controls and consequences of sulfate reduction rates in recent marine sediments, *in* Acid Sulfate Weathering. (J.A. Kittrick et al. eds.), Soil Sci. Soc. Amer. Special Report no. 10. p. 19-36.
Hem, J.D., Roberson, C.E., Lind, C.J., Polzer, W.L., 1973, Chemical interactions of aluminum with aqueous silica at 25° C; Chemistry of aluminum in natural waters: U.S. Geol. Surv. Water-Supply Paper 1827-E., 57p.
Henmi, T., and Wada K., 1976, Morphology and composition of allophane: Amer. Mineral., v.61, p.379-390.
Holdrige, D.A., and Vaughan, F., 1957, The kaolin minerals (kandites), *in* The differential thermal investigation of clays (R. C. Mackenzie, ed.): Mineralogical Society, London, 456p.
Keller, W.D., McGrain, P., Reesman, A.L., and Saum, N.M.,1966, Observations on the origin of endellite in Kentucky, and their extension to "indianite": Proc. 13th. Clays and Clay Miner. Conf., p. 107-120.
Kirkman, J.H., 1981, Morphology and structure of halloysite in New Zealand tephras: Clays and Clay Miner., v.29, p.1-9.
McGrain, P., 1966, Some sources of ceramic materials in Kentucky: Kentucky Geol. Surv., Series 10, No. 1., 25p.
McGrain, P., and Kendall, T.A., 1972, Miscellaneous analyses of Kentucky clays and shales for 1960-1970: Kentucky. Geol. Surv., Series 1O, No. 12, 62p.
Milton, C., Conant, L.C., and Swanson, V.E. 1955, Sub-Chattanooga residuum in Tennessee and Kentucky: Geol. Soc. Amer. Bull., v.66, p.806-810.
Nagasawa, K., and Miyazaki, S., 1976, Mineralogical properties of halloysite as related to its genesis: Proc. Int. Clay Conf. (S.W. Bailey, ed.), Mexico City, 1975, Applied Publishing, p.257-265.
Nagasawa, K., and Noro, H., 1987, Mineralogical properties of halloysites of weathering origin: Chemical Geology, v.60, p. 145-149.
Nordstrom, D.K., 1982, Aqueous pyrite oxidation and the consequent formation

of secondary iron minerals, *in* Acid sulfate weathering (J.A. Kittrick, D.S. Fanning, and L.R. Hosner,eds.): Soil Science Soc. Amer., p.37-56.
Okada, K., Morikawa, S., Iwai, S., Ohira, Y., and Kakuto, Y., 1975, A structure model of allophane: Clay Sci., v.4, p.29I- 303.
Parfitt, R.L., Firkut, R.J., and Henmi, T.,1980, Identification and structure of two types of allophane from volcanic ash soils and tephra: Clays and Clay Miner., v.28, p.328-334.
Rice, G., 1962, Silurian-Devonian stratigraphy of southern Madison, southern Garrard, and eastern Lincoln counties: unpublished M.S. thesis, University of Kentucky, 67p.
Ross, C.S., Kerr, F.E., 1934, Halloysite and allophane: U.S. Geol. Surv. Prof. Paper 185, p.135-148.
Shawe, F.R., and Wigley, P.B., 1974, Geologic map of the Stanford quadrangle, Boyle and Lincoln counties Kentucky: U.S. Geol. Surv. Geologic Quadrangle Map GQ-1137.
Singer, P.C., and Stumm, W., 1970, Acid mine drainage: the rate determining step: Science, v. 197, p. 1121-1123.
Stumm, W., and Morgen, J.J., 1981, Aquatic Chemistry, 2nd ed.: Wiley, New York, 780p.
Van der Gast, S.I., Wada, S.J., Wada, K., and Kakuto, Y., 1985, Small-angle x-ray powder diffraction, morphology, and structure of allophane and imogolite: Clays and Clay Miner. v.33, p.237-243.
van der Marel, H.W., and Beutelspacher, H., 1976, Altas of infrared spectroscopy of clay minerals and their admixtures: Elsevier, New York, 396p.
van Olphen, H.,1977, An introduction to clay colloid chemistry: for clay technologists, geologists and soil scientists: Wiley, New York, 318p.
Vuorinen, A, Hiltunen, P., Hsu J.C., and Tuovinen, O.H., 1983, Solubilization and speciation of iron during pyrite oxidation by Thiobacillus ferrooxidans: Geomicrobiol. J., v.3, p.95- 120.
Wada, K.,1977, Allophane and imogolite, In Minerals in Soil Environments (J.G. Dixon et al., eds.): Soil Sci. Soc. America, p.603-633.
Weaver, C.E., 1976, The nature of TiO in Kaolinite: Clays and Clay Minerals, v.24, p.215-218.
Weaver, C.E., 1980, Fine-grained rocks: shales or physilites: Sediment. Geol., v.27, p.301-313.
Williamson, I., 1970, Tonsteins- their nature, origins and uses: Mining magazine, v.122, p.119-211.
Wilson, E.N., and Sutton, D.G., 1973, Oil and gas map of Kentucky, Sheet 3, East-Central Part: Kentucky. Geol. Surv.

REGIONAL VARIATION IN METAMORPHIC CONDITIONS RECORDED BY PELITIC SCHISTS IN THE BALTIMORE AREA, MARYLAND

HELEN M. LANG

Department of Geology and Geography
West Virginia University
Morgantown, West Virginia 26506

ABSTRACT

Metasedimentary rocks that overlie the Baltimore Gneiss in the vicinity of Baltimore, Maryland, show evidence of having experienced only one major episode of metamorphism. Within the 25 X 20 km^2 kyanite zone north and west of Baltimore most pelitic rocks contain kyanite, which commonly coexists with staurolite and/or sillimanite. Garnet-biotite geothermometry and GASP and GRAIL geobarometry indicate that rocks within the kyanite zone experienced peak metamorphic conditions in the range of 520 to 600° C at 4.6 to 7.4 kilobars total pressure. Systematic variations in estimated temperature (T) and especially pressure (P) relate to the position of metapelite samples relative to exposures of Baltimore Gneiss. Samples from an inlier within the Phoenix Anticline of Baltimore Gneiss give the highest T and P estimates. Samples from the margin of Baltimore Gneiss exposures give intermediate P and T estimates, and samples from between Baltimore Gneiss exposures give the lowest T and P estimates. The systematic variations in estimated pressure at the peak of metamorphism can be reconciled with the schematic cross section of the Baltimore area by Fisher and others (1979) if metamorphism was essentially complete before refolding of Baltimore Gneiss-cored nappes. Nappe refolding would have raised rocks in anticline hinges, which experienced metamorphism at greater depths, relative to rocks in syncline hinges, which experienced metamorphism at shallower depths. Small amounts of late sillimanite in many samples (particularly those from the inlier in the Phoenix Anticline) indicate that those samples experienced a pressure decrease (and/or temperature increase) late during metamorphism. Late kyanite in the samples from between Baltimore Gneiss anticlines, which yield low pressure estimates, corroborates the assertion that those samples experienced a late increase in pressure.

INTRODUCTION

Rocks of the Appalachian Piedmont have experienced a complex geologic history, but are deeply weathered and poorly exposed. As a consequence, the Piedmont Geologic Province is perhaps the most poorly understood part of the Appalachian orogen (Fisher, 1970a). The position of the Piedmont between the folded and faulted rocks of the Valley and Ridge Province to the west and northwest and the suspect terranes to the east gives it a prominent role in tectonic models of the orogen (e.g., Thomas, 1977; Williams, 1978; Zen, 1981; Rodgers, 1982; Glover and others, 1983; Williams and Hatcher, 1983). In order to test and

refine models for the evolution of the Appalachians, we must know more about the details of the complex metamorphic and tectonic history recorded by rocks of the Piedmont.

A section through the entire Piedmont terrane from slightly metamorphosed rocks of the western Piedmont (Ijamsville phyllite) through high-grade basement gneisses (Baltimore Gneiss) is exposed in a narrow belt in eastern Maryland. The deepest part of the orogen is represented by the Baltimore Gneiss and metasedimentary rocks immediately adjacent to it. The quartzo-feldspathic Baltimore Gneiss contains few pressure- and temperature-sensitive mineral assemblages; however, pelitic rocks are common in the metasediments that overlie it. A thermobarometric study of pelitic rocks from the high-grade terrane in Baltimore County was undertaken to determine the metamorphic history of these rocks, which represent the deeper parts of the Appalachian Mountain Range.

GEOLOGIC SETTING

The geologic map pattern of the eastern Maryland Piedmont is dominated by the Baltimore Gneiss domes or anticlines (Figure 1; Crowley and others, 1976a;

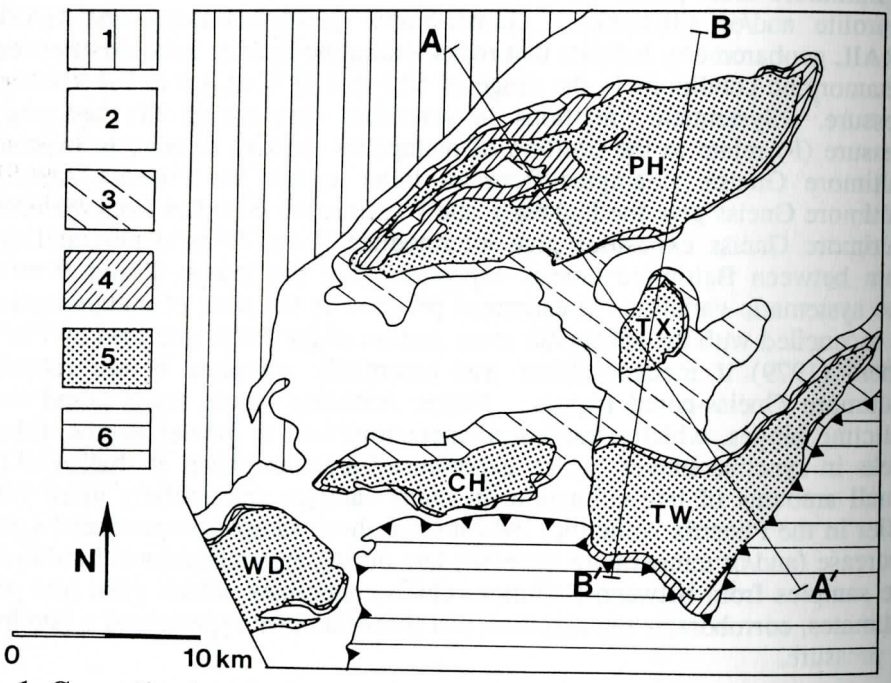

Figure 1. Generalized geologic map of Baltimore County and adjacent areas (after Crowley and others, 1976). 1 - Low- to medium-grade metasediments of the western Piedmont; 2 - Loch Raven Formation, mainly pelitic schist; 3 - Cockeysville Marble; 4 - Setters Formation, quartzite and pelitic schist; 5 - Baltimore Gneiss, felsic basement gneiss; 6 - Baltimore Mafic Complex, island arc complex that collided with the Baltimore Gneiss Terrane (Units 2-5) during the Taconic Orogeny (at approximately 470 Ma). Anticlines in which the Baltimore Gneiss is exposed are labeled PH=Phoenix, TX=Texas, TW=Towson, CH= Chattolanee, and WD=Woodstock Anticlines. The lines labeled A-A' and B-B' show the approximate locations of the schematic cross sections shown in Figure 2.

Cleaves and others, 1968). The quartzo-feldspathic Baltimore Gneiss that forms the cores of the anticlines is at least 1.0 to 1.1 billion years old (Crowley, 1976). Metasediments of the Glenarm Supergroup (Crowley, 1976) unconformably overlie the Baltimore Gneiss. The lowermost unit of the Glenarm Supergroup is the Setters Formation, which consists predominantly of flaggy, micaceous quartzite with abundant tourmaline along the partings. The garnet schist member of the Setters Formation, which commonly contains abundant kyanite and/or staurolite (Fisher, 1971a) is a discontinuous unit toward the top of the Setters Formation. The Setters Formation is overlain by the relatively clean Cockeysville Marble, which is in turn overlain by the Loch Raven Formation (Crowley, 1976; Crowley and others, 1976a). Crowley and others (1976a) include the Loch Raven Formation, which consists primarily of pelitic schist, in the Wissahickon Group; however, Drake (1985, 1986) has recognized problems with stratigraphic correlation and nomenclature in the Wissahickon Group in the course of his work in northern Virginia. The Setters garnet schist and the Loch Raven schist are of primary interest in this study, because they are uniformly pelitic in composition and commonly contain garnet, staurolite, and/or kyanite.

Geologic maps (at 1:62500) of Montgomery (Cloos and Cooke, 1953), Howard (Cloos and Broedel, 1940), Baltimore (Crowley and others, 1976a) and Harford (Southwick and Owens, 1968) Counties cover most of the eastern Maryland Piedmont. Recent work by geologists at the Maryland Geological Survey has produced 7 1/2 minute geologic quadrangle maps (at 1:24000) for most of Baltimore County (Muller, 1985; Moller, 1979; Crowley and others, 1975; Crowley and Cleaves, 1974; Crowley and others, 1976b; Crowley, 1977; Crowley and Reinhardt, 1979, 1980; Reinhardt and Crowley, 1979). These maps provide an excellent basis for more detailed studies such as the one reported here.

Recent geophysical studies (Fisher and others, 1979; Muller and Chapin, 1984) have shown that the Baltimore Gneiss forms the cores of one or more westward directed, complexly refolded nappes (See Figure 2 for schematic cross sections). Muller and Chapin (1984) found evidence for three periods of deformation that affected the Baltimore Gneiss. The first period, D_1 (Grenville age 1000-1200 m.y.) affected only the Gneiss and is enigmatic. The second protracted period of deformation (D_2), which also affected overlying metasediments, produced three generations of folds designated F_{2_a} (nappe-stage folds), F_{2_b} (folds with near-vertical axial planes that refolded the nappes), and F_{2_c} (folds that locally refolded F_{2_b} folds). D_2 deformation was contemporaneous with the major period of metamorphism (Muller and Chapin, 1984; Hall and Lang, 1987; Hall, 1988). Muller and Chapin (1984) proposed that D_2 spanned the Taconic and Acadian orogenies. Age of metamorphism and D_2 deformation is, however, problematic. A 458 million year age for the post-tectonic Ellicott City pluton (Sinha, 1988) indicates that terrane accretion had occurred by the end of the Taconic orogeny; however, an isotopic study in northern Virginia by Sutter and others yields Alleghanian cooling ages for rocks in that part of the Piedmont (Sutter and others, 1985; Sutter, personal communication, 1987). The third, relatively minor, deformational episode, D_3, resulted in predominantly brittle faulting and open folding. D_3 may have been contemporaneous with localized retrograde metamorphism. Muller and Chapin's (1984) model provides an excellent framework for further detailed studies of crystalline rocks of the Maryland Piedmont.

General information about metamorphism in the eastern Maryland Piedmont

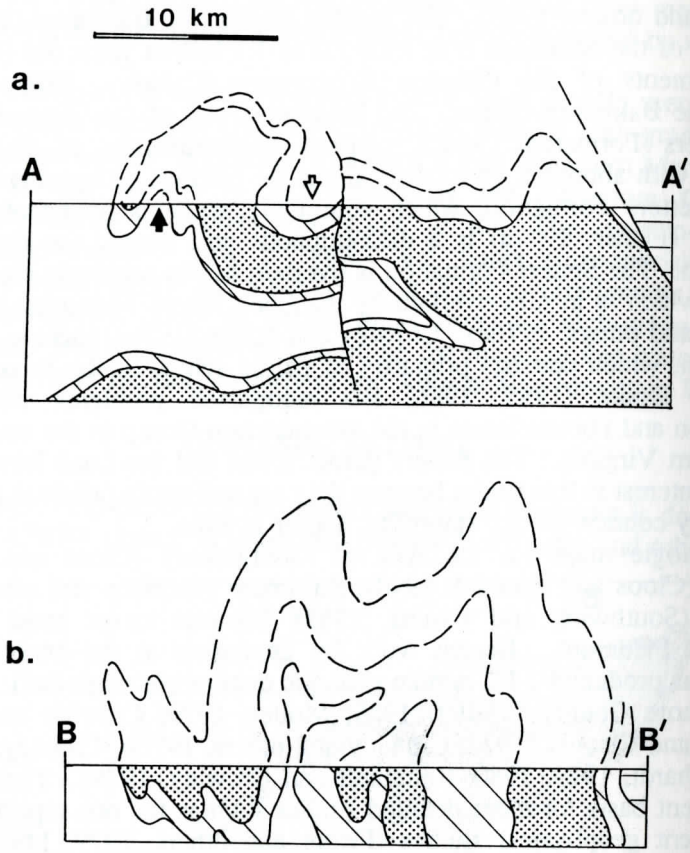

Figure 2. Schematic cross sections through the Baltimore area. (a.) A-A' (see Figure 1) cross section after Fisher and others, 1979, and (b.) B-B' (see Figure 1) cross section after Muller and Chapin, 1984. The stippled pattern represents the Baltimore Gneiss; the diagonal line pattern represents the Cockeysville and Setters Formations combined; the unpatterned area is the Loch Raven Formation and the horizontal line pattern represents the Baltimore Mafic Complex. The open and filled arrows on (a.) are referred to in the text.

is contained in county geologic reports (Hopson, 1964; Southwick, 1968; Crowley, 1976); however, few detailed studies of metamorphism in the area have been done. Fisher (1970b, 1971b) studied rocks on Bear Island in the Potomac River. Because these rocks are not very pelitic and have been affected by retrograde metamorphism, he was not able to deduce detailed information about metamorphic conditions from them. A brief note about staurolite-kyanite bearing rocks in the Setters Formation (Fisher, 1971a) and a study of migmatites in the Baltimore Gneiss (Olsen, 1977) are the only additional studies of metamorphism in the eastern Maryland Piedmont. Only very general estimates of metamorphic conditions based on phase equilibria were made in these studies (Fisher 1971b; Olsen, 1977). No quantitative estimates based on calibrated thermobarometers have been made, nor have there been any attempts to document changes in metamorphic conditions within the Baltimore area. A few detailed studies of metamorphic rocks from similar settings in the Pennsylvania and northern Virginia Piedmont have been reported (Crawford and Mark, 1982; Flohr and Pavlides, 1986).

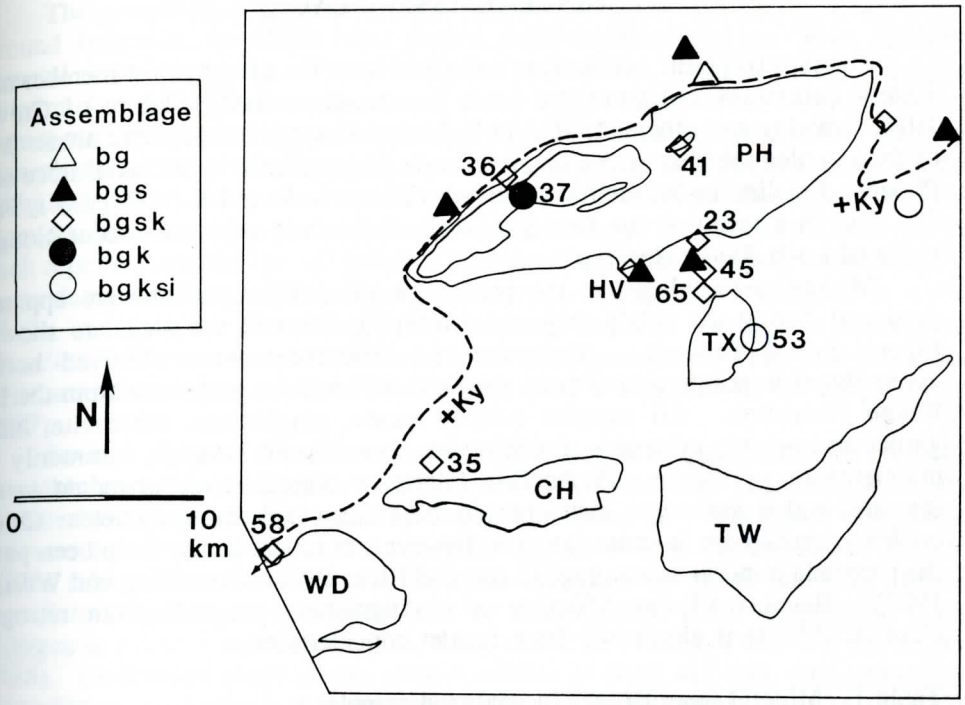

Figure 3. Metamorphic assemblage map for the Baltimore area. Symbols indicate the AFM assemblages as shown on the Figure (b=biotite, g=garnet, s=staurolite, k=kyanite, si=sillimanite). All samples contain muscovite, quartz, plagioclase, ilmenite ±magnetite ±pyrrhotite. The heavy dashed line is a generalized regional kyanite isograd (+Ky on the high-grade side). Areas underlain by Baltimore Gneiss are shown for reference (PH=Phoenix, TX=Texas, TW=Towson, CH=Chattolanee and WD=Woodstock Anticlines). The number of each analyzed sample is shown near the symbol that represents its assemblage (all numbers have the prefix MD). HV on the map indicates the location of the large Hunt Valley Mall exposure where two different assemblages (indicated by appropriate symbols) have been collected.

There is evidence for only one major metamorphic episode in the metapelites of Baltimore County, although Fisher (1970b, 1971b) saw evidence for multiple metamorphic events further south at Great Falls of the Potomac River. While lack of exposure and appropriate rock composition prevents mapping of detailed isograds in most of the eastern Maryland Piedmont, it was recognized early that highest grade metamorphic assemblages are exposed nearest the Baltimore Gneiss (Hopson, 1964). Doe, Tilton and Hopson (1965) mapped generalized staurolite and kyanite isograds for the entire Baltimore area (see also the Geologic Map of Maryland, Cleaves and others, 1968). Southwick and Owens (1968) mapped isograds in some detail in the southwestern part of Harford County. Crowley and others (1976a) and Crowley (1976) recognized several "facies" of the Loch Raven schist (garnet, staurolite, garnet-staurolite, garnet-kyanite, and garnet-staurolite-kyanite facies) and indicated them on the geologic map of Baltimore County. A generalized regional kyanite isograd, based on these studies and work related to this study, is shown in Figure 3.

MINERAL ASSEMBLAGES

Samples of pelitic schist were collected from the garnet schist member of the Setters Formation and from the Loch Raven schist (nomenclature of Crowley, 1976; Crowley and others, 1976a) in Baltimore County and adjacent areas. Many of the samples are clustered along a traverse perpendicular to the axial trace of the Phoenix anticline in the vicinity of cross sections A-A' and B-B' (Figure 1, Figure 3). This is a result of the fact that some of the best exposures occur along the shore of Loch Raven Reservoir.

Mineral assemblages in the pelitic samples, all of which were apparently produced during the single major metamorphic event in the area, are shown in Figure 3 and Table 1. No systematic differences were observed between assemblages in pelitic schists from the Setters Formation and those from the Loch Raven Formation. All samples contain quartz, plagioclase, muscovite, biotite, garnet and opaque minerals. Ilmenite was found in all samples, commonly with magnetite or pyrrhotite. Plagioclase (albite or oligoclase) is abundant in most samples, and it commonly forms porphyroblasts up to 3 cm in diameter. Chlorite is clearly retrograde in some samples; however, in others it may have been part of the prograde mineral assemblage (Lang and Rice, 1985a; Grambling and Williams, 1987). Because of the difficulty of distinguishing prograde from retrograde chlorite, chlorite is eliminated from further consideration.

Table 1. Mineral assemblages in analyzed samples.

SAMPLE NUMBER (arranged North to South)	Chl	Bt	Grt	St	Ky	Sil	Mag	Ilm	Rt	Po
MD36*	X	X	X	X	X	m+	X	X		
MD37		X	X		X			X	X	
MD41		X	X	X	X	m	X	X	?	
MD23	X	X	X	X	X	m		X	X	
HV# HV8		X	X	X	X	m		X	X	
HV10		X	X	X	X	m		X	m	X
HV101		X	X	X	X	m		X	X	X
HV104	X	X	X	X	X	m		X	X	X
HV106		X	X	X	X	m		X	X	X
MD22	X	X	X	X	X	m		X	X	X
MD45		X	X	X	X		X	X		
MD65	X	X	X	X	X		X	X		
MD53		X	X	m	X	X	?	X		
MD35		X	X		X	m		X	X	X
MD58	X	X	X	X	X			X	m	

* Samples are arranged in approximate order from north to south. All samples contain muscovite, quartz and plagioclase in addition to the minerals indicated in the Table.

\+ m indicates the occurrence of a few small crystals of sequestered Zn-rich staurolite (if in the Sta column), a few fine prisms of late sillimanite in the sample (if in the Sil column) or minor rutile (if in the Rt column).

\# Indented HV samples (and MD22) all come from the same 500 meter-long exposure at Hunt Valley Mall in Cockeysville, Maryland.

The generalized regional kyanite isograd of Figure 3 encloses a large area around Baltimore in which most pelitic rocks contain kyanite. Five different mineral assemblages have been observed within the regional kyanite isograd (Figure 3). AFM phases constituting these assemblages are as follows: biotite-garnet-staurolite; biotite-garnet-staurolite-kyanite; biotite-garnet-kyanite (without staurolite); biotite-garnet-staurolite-kyanite-sillimanite; and biotite-garnet-kyanite-sillimanite. Because these minerals are porphyroblastic and commonly isolated from one another, three-phase contacts among them are not common; however, for each reported assemblage, all possible two phase contacts have been observed and no evidence of disequilibrium has been observed. Sillimanite is included as a part of the metamorphic assemblage only in those samples where it is coarse and abundant. Many other samples contain small amounts of fine, post-kinematic sillimanite that apparently formed late in the P-T-t evolution of the rocks (Lang, 1987).

Several factors contribute to the fact that the distribution of mineral assemblages within the kyanite isograd is not very systematic: (1) much of the area is underlain by quartz-rich rock (Rush Brook member of Loch Raven Formation) and marble, which do not contain diagnostic assemblages, (2) exposures of fresh pelitic schist are uncommon even in areas underlain by pelitic units, (3) minor variations in pelitic rock compositions or metamorphic fluid composition cause changes in mineral assemblage (c.f., Lang and Rice, 1985a; Tracy and Robinson, 1988). (A detailed study of the relative effects of fluid and bulk composition on staurolite vs. staurolite-kyanite assemblages at one large exposure in the area (HV in Figure 3) is in progress (Lang, in preparation).) Even so, rocks exposed between the Phoenix and Chattolanee-Towson anticlines (Figure 3) all seem to have experienced metamorphism at a similar level in the crust. Thermobarometric techniques were applied in order to determine whether pressure or temperature gradients could be detected within this (25 x 20 km^2) kyanite zone. Numbers of samples chosen for microprobe analysis are shown on Figure 3 and their mineral assemblages are summarized in Table 1.

MICROPROBE ANALYSIS

Mineral compositions were determined by analyzing carbon-coated, polished thin sections on the ARL-SEMQ microprobe at Virginia Polytechnic Institute and State University. Operating conditions were 15 keV accelerating potential and 20 na beam current. A focussed beam ~1um in diameter was used for garnet and other minerals in which volatile loss was not likely to be a problem. A 4x4um raster was used for micas and plagioclase to avoid loss of volatile elements. Standard nine-element analyses were done for most minerals. Eighteen element analyses (Solberg and Speer, 1982) were done on a few staurolites, biotites, and muscovites in each sample in order to determine Zn, F, and detect other minor elements. Well-characterized natural standards were used for most elements; synthetic oxide or glass standards were used for a few minor elements. Data reduction was performed according to the procedure of Bence and Albee (1968) with the alpha factors of Albee and Ray (1970). All iron is reported as FeO.

Quartz, kyanite, and sillimanite were assumed to be pure. Other major minerals (biotite, garnet, staurolite, plagioclase, muscovite, ilmenite, magnetite, and sulfide) in samples from the nine localities shown in Figure 3 plus six kyanite-bearing samples from the long exposure at Hunt Valley Mall (HV in Figure 3) were

analyzed. Five to six spots on each mineral in each sample were analyzed. Average mineral compositions are summarized in Table 2.

Table 2. Summary of mineral composition data.

	GARNET COMPONENTS				BIOTITE		PLAGIOCLASE			MUSCOVITE		ILMENITE
	X-Alm	X-Prp	X-Grs	X-Sps	Mg/vi*	Fe/vi	X(An)	X(Ab)	X(Or)	Na/Na+K	Alvi#/vi	Ilm/Ilm+Hem
MD36	0.733	0.154	0.070	0.042	0.512	0.340	0.249	0.748	0.000	0.211	0.873	
MD37	0.796	0.150	0.038	0.015	0.435	0.396				0.145	0.892	0.97
MD41	0.734	0.153	0.038	0.075	0.449	0.376	0.147	0.851	0.003	0.176	0.879	
MD23	0.819	0.133	0.034	0.014	0.413	0.407	0.144	0.853	0.003	0.200	0.913	1.00
HV8	0.757	0.162	0.064	0.017	0.465	0.359	0.263	0.733	0.004	0.177	0.888	1.00
HV10	0.747	0.161	0.070	0.023	0.451	0.360	0.290	0.707	0.003	0.157	0.892	1.00
HV101	0.750	0.164	0.051	0.035	0.462	0.343	0.229	0.767	0.004	0.168	0.905	1.00
HV104	0.778	0.156	0.050	0.016	0.447	0.381	0.225	0.771	0.003	0.170	0.906	1.00
HV106	0.751	0.165	0.045	0.039	0.460	0.362	0.195	0.802	0.003	0.175	0.904	1.00
MD22	0.778	0.139	0.066	0.016	0.425	0.400	0.251	0.743	0.007	0.162	0.897	0.95
MD45	0.650	0.163	0.043	0.145	0.561	0.287	0.206	0.791	0.000	0.209	0.873	
MD65	0.650	0.164	0.053	0.134	0.537	0.301	0.210	0.787	0.003	0.220	0.873	
MD53	0.800	0.126	0.062	0.012	0.388	0.419	0.284	0.711	0.004	0.103	0.900	
MD35	0.778	0.135	0.041	0.046	0.419	0.400	0.162	0.835	0.003	0.158	0.913	0.98
MD58	0.792	0.121	0.069	0.018	0.434	0.390	0.198	0.798	0.004	0.205	0.923	

* vi indicates the calculated sum of the six-fold cations
\# Alvi indicates six-fold Al calculated on the basis of four tetrahedral Al+Si per formula unit

GEOTHERMOMETRY AND GEOBAROMETRY

All minerals in apparent textural equilibrium in a single (22x45mm) thin section are presumed to have reached equilibrium at some time during metamorphism. Because reactions proceed most rapidly at high temperature, it is probable that minerals equilibrated at the highest temperature attained during metamorphism (Spear and others, 1984). Textural equilibrium is supported when there is no evidence of reaction at points of contact between minerals, no minerals rim or replace other minerals, and grain boundaries are sharp, smooth and polygonal. Mineral assemblages chosen for microprobe analysis (Figure 3 and Table 1) generally fulfill these criteria. Complete equilibrium requires constant mineral composition within grains and among grains of a thin section. Some garnet porphyroblasts are strongly zoned (Lang, 1987, and in preparation), but no other significant variation in composition of a given mineral was observed within a thin section. Garnet rims are assumed to have been in equilibrium with matrix phases, because the temperature was not high enough for diffusion in garnet to have been very effective (Tracy, Robinson and Thompson, 1976).

Geothermobarometry was applied to appropriate assemblages in order to provide estimates of temperature and pressure at which minerals in the samples equilibrated. Garnet-biotite geothermometry (Ferry and Spear, 1978; Hodges and Spear, 1982; Ganguly and Saxena, 1984; Lang and Rice, 1985b), which is based upon the exchange of Fe and Mg between garnet and biotite:

1/3 Pyrope + 1/3 Annite = 1/3 Almandine + 1/3 Phlogopite

was used to estimate temperature. Activity-composition relationships proposed by Newton and Haselton (1981) and modified by Hodges and Spear (1982) were used for garnet, and biotite was assumed to be ideal (for comparison of garnet models, see Lang and Rice, 1985b). Temperature estimates at 6 kbar pressure (preliminary estimate of the average pressure) based on the garnet-biotite geothermometer are shown in Table 3. Temperature estimates for six kyanite-

Table 3. Temperature and pressure estimates for kyanite-bearing samples.

SAMPLE NUMBER (arranged North to South)	T(G-B) (°C, at 6kbar)	P(GASP) (kbar)*	P(GRAIL) (kbar)*
MD36	530	5.8	---
MD37	590	---	7.0
MD41	590	7.1	---
MD23	560	6.1	7.4
HV8	580	6.3	6.1
HV10	600	6.6	5.9
HV101	570	5.8	5.9
HV104	600	6.4	6.7
HV106	590	6.4	6.0
MD22	590	6.7	6.6
HV**	590	6.4	6.2
MD45	520	4.6	---
MD65	530	5.4	---
MD53	590	6.1	---
		6.1(s)	
MD35	580	6.5	6.6
MD58	540	6.5	---

* Kyanite is the Al_2SiO_5 polymorph unless otherwise indicated (s=sillimanite)

** HV is the average of all samples from Hunt Valley Mall.

bearing samples from the Hunt Valley Mall exposure and their average are included in the Table. These estimates indicate the range of variability in estimated temperature for samples that presumably equilibrated at the same metamorphic conditions.

Total pressure was estimated on the basis of the garnet, aluminosilicate, quartz, plagioclase (GASP) and garnet, rutile, aluminosilicate, ilmenite, quartz (GRAIL) geobarometers. The GASP geobarometer (Ghent, 1976; Newton and Haselton, 1981) is based on equilibrium among garnet, aluminosilicate, quartz and plagioclase according to the reaction:

3 Anorthite = Grossular + Al_2SiO_5 (Ky or Sil) + 2 Quartz

Activity-composition relationships for minerals involved in this equilibrium were taken from a review of the GASP geobarometer by Newton and Haselton (1981; with the garnet model as modified by Hodges and Spear, 1982). The more recent calibration of the GASP equilibrium by Koziol and Newton (1988) was used for the pressure estimate. Pressure of the GASP equilibrium, adjusted for composition of the minerals, at the garnet-biotite temperature for each sample with the appropriate assemblage is given in Table 3.

The GRAIL geobarometer (Bohlen and others, 1983; Ghent and Stout, 1984) was applied to those samples that contain the mineral assemblage garnet, rutile, aluminosilicate, ilmenite, quartz. This geobarometer, based on the equilibrium:

3 Ilmenite + Al_2SiO_5 + Quartz = Almandine + 3 Rutile

was calibrated by Bohlen and others (1983) and its application to pelitic rocks was discussed by Lang and Rice (1985b). The equation of Ghent and Stout (1984) was used, and activity of almandine was calculated on the basis of the aforementioned model for garnet (Newton and Haselton, 1981; Hodges and Spear, 1982). All minerals involved in the equilibrium other than garnet are essentially pure. The GRAIL pressure estimates, which represent the pressure of the adjusted GRAIL equilibrium at the garnet-biotite temperature for each sample, are given for appropriate samples in Table 3. For those samples to which both of the geobarometers can be applied, results are remarkably consistent.

The intersections of adjusted GASP or GRAIL equilibria with the garnet-biotite equilibrium for all of the samples (Figure 4) plot in the kyanite field as would be expected considering that all samples contain significant amounts of coarse-grained kyanite. The intersections are not far above the kyanite-sillimanite boundary and MD53, which contains coarse and abundant sillimanite in addition to kyanite plots closest to the sillimanite field (see the arrow in Figure 4).

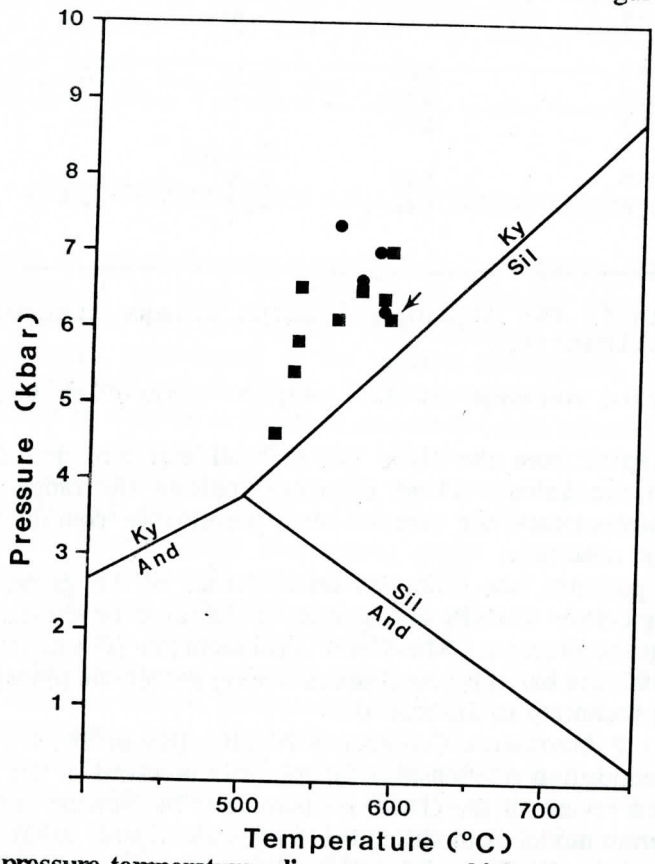

Figure 4. A pressure-temperature diagram on which the thermobarometric estimates of metamorphic conditions are plotted. Filled squares represent the intersection of the garnet-biotite geothermometer with the GASP geobarometer. Filled circles represent the intersection of the garnet-biotite geothermometer with the GRAIL geobarometer. All of the samples contain kyanite. The arrow indicates the pressure-temperature estimate for sample MD53, which contains abundant sillimanite in addition to kyanite. Al_2SiO_5 relations according to Holdaway (1971) are included for reference (And=andalusite, Ky=kyanite, Sil=sillimanite).

Although there are large uncertainties in the absolute values of the pressure estimates based on these geobarometers (see Lang and Rice, 1985b, and Hodges and McKenna, 1987, for discussion of uncertainties in geothermobarometry), changes in estimated pressure between samples are likely to be significant. The highest pressure estimates come from samples MD41(GASP) and MD37(GRAIL) from the inlier within the Phoenix Anticline and from MD23(GRAIL high, GASP intermediate), which lies directly adjacent to the Gneiss of the Phoenix Anticline. The lowest temperature and especially pressure estimates come from samples that lie between the Phoenix and Texas Anticlines (MD45 and MD65) and to the north of the Phoenix Anticline (MD36), where metamorphic grade drops off abruptly.

DISCUSSION

The estimated pressures, which represent conditions at the time of equilibration of garnet rims with matrix minerals, can be reconciled with the schematic cross-section of Fisher and others (1979; see Figure 2a) if metamorphism was essentially complete before refolding (D_{2_b} of Muller and Chapin, 1984) of the Phoenix nappe. Pressure estimates and field observations by the author are not easily reconciled with the schematic cross-section of Muller and Chapin (1984; Figure 2b). Rocks that equilibrated at very different depths (MD37 and MD41 at ~20 km; MD45 and MD65 at ~15 km) after nappe emplacement (D_{2_a}) could have been brought to a similar level in the crust (Figure 2a) by refolding before uniform uplift and erosion began. If a relatively flat-lying nappe were refolded into upright folds with east-west axes, rocks like MD41 and MD37 at anticline hinges would be brought from beneath the nappe to relatively shallower levels (filled arrow in Figure 2a) and rocks like MD45 and MD65 from syncline hinges would be brought to relatively deeper levels (open arrow in Figure 2a). Rocks in the limbs of D_{2_b} folds would have experienced less change in depth as a result of refolding and would give intermediate pressure estimates (as do MD53 and most HV samples). Detailed study of textural relationships in samples from the one locality at which they have been examined in detail (HV in Figure 3) indicate that metamorphic mineral growth began before nappe refolding and continued during refolding (Hall, 1988; Hall and Lang, 1987). Partial reequilibration of garnet rims with matrix phases during refolding may have affected geothermobarometry so that pressure-temperature estimates do not reflect the most extreme conditions reached by a given sample.

Textural relationships in some of the samples support the hypothesis that some rocks experienced a decrease in pressure late during metamorphism, while others experienced a late increase in pressure. Sample MD41 contains abundant coarse-grained kyanite, which is in apparent textural equilibrium with garnet, biotite, plagioclase and minor staurolite. This sample also contains a small cluster of very fine, elongate, clear prisms (Figure 5a) at a garnet-plagioclase boundary that are apparently fibrolitic sillimanite (see Vernon and Flood (1977) for interpretation of fibrolite textures). Some samples from D_{2_b} fold limbs also contain a small amount of fine clear sillimanite prisms (MD22, most HV samples, MD23, MD35). In contrast, MD45 and MD65 contain small clusters of small, dark, stubby prisms that appear to be late kyanite rather than sillimanite (Figure 5b). All of these clusters of fine, late aluminosilicate minerals occur within or at the margins of aluminous minerals such as garnet or plagioclase. The presence of late aluminosilicates suggests that some cation exchange, which would affect the

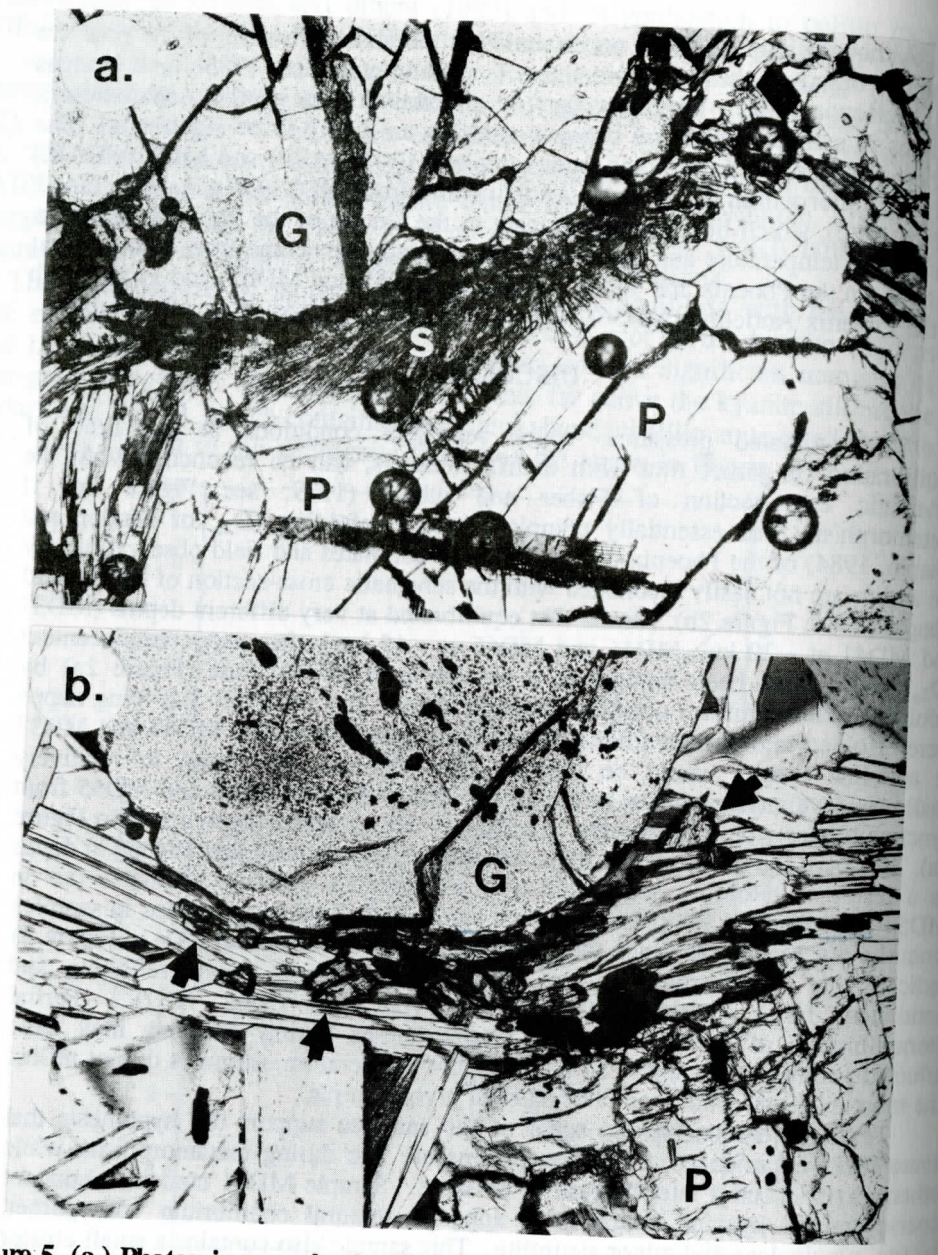

Figure 5. (a.) Photomicrograph of a cluster of fine, clear, elongate prisms in sample MD41, which are presumed to be late, postkinematic sillimanite. Coarse-grained kyanite is abundant elsewhere in the sample. (Plane-polarized light; the long dimension of the photograph is 1.7mm. G=garnet, P=plagioclase, S=sillimanite.) (b.) Photomicrograph of a cluster of dark, stubby prisms of late, postkinematic kyanite in sample MD45 (see black arrows on Figure). Coarse-grained kyanite occurs elsewhere in the thin section. (Plane-polarized light; the long dimension of the photograph is 1.7mm. G=garnet, P=plagioclase, K=kyanite.)

geothermobarometry, may have occurred late in the metamorphic sequence during nappe refolding.

CONCLUSIONS

(1) Metasedimentary rocks that overlie the Baltimore Gneiss in the vicinity of Baltimore, Maryland, show evidence of having experienced only one major episode of metamorphism.
(2) Although exposure is limited and distribution of mineral assemblages is not very systematic, there is a large kyanite zone (approximately 25 X 20 km^2) north and west of Baltimore in which most pelitic rocks contain kyanite, which commonly coexists with staurolite and/or sillimanite.
(3) Garnet-biotite geothermometry and GASP and GRAIL geobarometry indicate that rocks within the kyanite zone experienced peak metamorphic conditions in the kyanite field in the range of 520 to 600° C at 4.6 to 7.4 kilobars total pressure.
(4) There are systematic variations in estimated temperature (T) and especially pressure (P) that relate to the position of metapelite samples relative to exposures of Baltimore Gneiss. Samples from an inlier within the Phoenix Anticline of Baltimore Gneiss give the highest T and P estimates. Samples from the margin of the Baltimore Gneiss exposures give intermediate P and T estimates and samples from between Baltimore Gneiss exposures give the lowest T and P estimates.
(5) The systematic variations in estimated pressure (and depth) at the peak of metamorphism can be reconciled with the schematic cross section of the Baltimore area by Fisher and others (1979) if metamorphism was essentially complete before refolding of the Gneiss-cored nappes. Subsequent nappe refolding would have raised rocks in anticline hinges that experienced metamorphism at greater depths relative to other rocks in syncline hinges that experienced metamorphism at shallower depths. Textural relationships are generally consistent with this interpretation.
(6) Small amounts of late sillimanite in many samples (particularly those from the inlier in the Phoenix Anticline) indicate that they experienced a pressure decrease (and/or temperature increase) late during metamorphism. Late kyanite in the samples from between Baltimore Gneiss anticlines that give low pressure estimates corroborates the assertion that they experienced a late increase in pressure.

ACKNOWLEDGEMENTS

I would like to thank Peter Muller, Jonathan Edwards and George Fisher for valuable discussions of Maryland Piedmont geology, Peter Muller, Jonathan Edwards and Pam Hall for assistance in the field, and Lincoln Hollister for a helpful review. Todd Solberg provided valuable assistance with the microprobe. Financial support was provided by NSF Grant EAR-8721034 and a West Virginia University Faculty Senate Research Grant.

REFERENCES CITED

Albee, A.L. and Ray, L., 1970, Correction factors for electron microanalysis of silicates, oxides, carbonates, phosphates and sulfates: Analytical Chemistry, v. 42, p. 1408-1414.
Bence, A.E. and Albee, A.L., 1968, Empirical correction factors for the electron

microanalysis of silicates and oxides: Journal of Geology, v. 76, p. 382-403.
Bohlen, S.R., Wall, V.J. and Boettcher, A.L., 1983, Experimental investigations and geological applications of equilibria in the system FeO-TiO_2-Al_2O_3-SiO_2-H_2O: American Mineralogist, v. 68, p. 1049-1058.
Cleaves, E.T., Edwards, J., Jr. and Glaser, J.D., 1968, Geologic map of Maryland: Maryland Geological Survey.
Cloos, E. and Broedel, C.H., 1940, Geologic map of Howard County: Maryland Geological Survey.
Cloos, E. and Cooke, C.W., 1953, Geologic map of Montgomery County and the District of Columbia: Maryland Geological Survey.
Crawford, M.L. and Mark, L.E., 1982, Evidence from metamorphic rocks for over-thrusting, Pennsylvania Piedmont, U.S.A.: Canadian Mineralogist, v. 20, p. 333-347.
Crowley, W.P., 1976, The geology of the crystalline rocks near Baltimore and its bearing on the evolution of the eastern Maryland Piedmont: Maryland Geological Survey Report of Investigations No. 27.
Crowley, W.P., 1977, Geologic map of the Reisterstown Quadrangle, Maryland: Maryland Geological Survey.
Crowley, W.P. and Cleaves, E.T., 1974, Geologic map of the Towson Quadrangle, Maryland: Maryland Geological Survey.
Crowley, W.P. and Reinhardt, J., 1979, Geologic map of the Baltimore West Quadrangle, Maryland: Maryland Geological Survey.
Crowley, W.P. and Reinhardt, J., 1980, Geologic map of the Ellicott City Quadrangle, Maryland: Maryland Geological Survey.
Crowley, W.P., Reinhardt, J. and Cleaves, E.T., 1975, Geologic map of the Cockeysville Quadrangle, Maryland: Maryland Geological Survey.
Crowley, W.P., Reinhardt, J. and Cleaves, E.T., 1976a, Geologic map of Baltimore County and City: Maryland Geological Survey.
Crowley, W.P., Reinhardt, J. and Cleaves, E.T., 1976b, Geologic map of the White Marsh Quadrangle, Maryland: Maryland Geological Survey.
Doe, B.R., Tilton, G.R. and Hopson, C.A., 1965, Lead isotopes in feldspars from selected granitic rocks associated with regional metamorphism: Journal of Geophysical Research, v. 70, p. 1947-1968.
Drake, A.A., Jr., 1985, Tectonic implications of the Indian Run Formation—a newly recognized sedimentary melange in the northern Virginia Piedmont: U.S. Geological Survey Professional Paper 1324, 12 p.
Drake, A.A., 1986, Probable Late Proterozoic rocks of the Central Appalachian Piedmont: Geological Society of America Abstracts with Programs, v. 18, p. 14.
Ferry, J.M. and Spear, F.S., 1978, Experimental calibration of the partitioning of Fe and Mg between biotite and garnet: Contributions to Mineralogy and Petrology, v. 66, p. 113-117.
Fisher, G.W., 1970a, Introduction to Section IV: The Piedmont: *In* Fisher, G.W., Pettijohn, F.J., Reed, J.C., Jr., and Weaver, K.N. (ed.) Studies in Appalachian Geology: Central and Southern, Interscience, New York, p. 295-298.
Fisher, G.W., 1970b, The metamorphosed sedimentary rocks along the Potomac River near Washington, D.C., *in* Fisher, G.W., Pettijohn, F.J., Reed, J.C., Jr., Weaver, K.N. (ed.) Studies in Appalachian Geology: Central and Southern,

Interscience, New York, p. 299-316.
Fisher, G.W., 1971a, Kyanite- staurolite- and garnet-bearing schists in the Setters Formation, Maryland Piedmont: Geological Society of America Bulletin, v. 82, p. 229-232.
Fisher, G.W., 1971b, The Piedmont crystalline rocks at Bear Island, Potomac River, Maryland: Maryland Geological Survey Guidebook No. 4, 32 p.
Fisher, G.W., Higgins, M.W. and Zietz, I., 1979, Geological interpretations of aeromagnetic maps of the crystalline rocks in the Appalachians, northern Virginia to New Jersey: Maryland Geological Survey Report of Investigations No. 32.
Flohr, M.J.K. and Pavlides, L., 1986, Thermobarometry of schists from the Quantico Formation and the Ta River metamorphic suite, Virginia: Geological Society of America Abstracts with Programs, v. 18, p. 221.
Ganguly, J. and Saxena, S.K., 1984, Mixing properties of alumino-silicate garnets: constraints from natural and experimental data, and applications to geothermobarometry: American Mineralogist, v. 69, p. 88-97.
Ghent, E.D., 1976, Plagioclase-garnet-Al_2SiO_5-quartz: a potential geobarometer-geothermometer: American Mineralogist, v. 61, p. 710-714.
Ghent, E.D. and Stout, M.Z., 1984, TiO_2 activity in metamorphosed pelitic and basic rocks: principles and applications to metamorphism in southeastern Canadian Cordillera: Contributions to Mineralogy and Petrology, v. 86, p. 248-255.
Glover, L., III, Speer, J.A., Russell, G.S. and Farrar, S.S., 1983, Ages of regional metamorphism and ductile deformation in the central and southern Appalachians: Lithos, v. 16, p. 223-245.
Grambling, J.A. and Williams, M.L., 1987, Manganese and the appearance of an "extra" AFM phase in low-variance, 500° C rocks at Pecos Baldy, N.M.: Geological Society of America Abstracts with Programs, v. 19, p. 681.
Hall, P.S., 1988, Deformation and metamorphism of the aluminous schist member of the Setters Formation, Cockeysville, Maryland: Unpublished M.S. thesis, West Virginia University, Morgantown, W.V., 99p.
Hall, P. and Lang, H.M., 1987, Metamorphism and deformation of the Setters Formation, MD: Geological Society of America Abstracts with Programs, v. 19, p. 88.
Hodges, K.V. and McKenna, L.W., 1987, Realistic propagation of uncertainties in geologic thermobarometry: American Mineralogist, v. 72, p. 671-680.
Hodges, K.V. and Spear, F.S., 1982, Geothermometry, geobarometry and the Al_2SiO_5 triple point at Mt. Moosilauke, New Hampshire: American Mineralogist, v. 67, p. 1118-1134.
Holdaway, M.J., 1971, Stability of andalusite and the aluminum silicate phase diagram: American Journal of Science, v. 271, p. 97-131.
Hopson, C.A., 1964, The crystalline rocks of Howard and Montgomery Counties: *in* The Geology of Howard and Montgomery Counties, Maryland Geological Survey, p. 27-215.
Koziol, A.M. and Newton, R.C., 1987, Redetermination of the anorthite breakdown reaction and improvement of the plagioclase-garnet-Al_2SiO_5-quartz geobarometer: American Mineralogist, v. 73, p. 216-223.
Lang, H.M., 1987, Evidence from garnet zoning for overthrusting in the Eastern Maryland Piedmont: Geological Society of America Abstracts with Programs, v. 19, p. 24.

Lang, H.M. and Rice, J.M., 1985a, Regression modelling of metamorphic reactions in metapelites, Snow Peak, northern Idaho: Journal of Petrology, v. 26, p. 857-887.

Lang, H.M. and Rice, J.M., 1985b, Geothermometry, geobarometry and T-X(Fe-Mg) relations in metapelites, Snow Peak, northern Idaho: Journal of Petrology, v. 26, p. 889-924.

Moller, S.A., 1979, Geologic map of the Phoenix Quadrangle, Maryland: Maryland Geological Survey.

Muller, P.D., 1985, Geologic Map of the Hereford Quadrangle, Maryland: Maryland Geological Survey.

Muller, P.D. and Chapin, D.A., 1984, Tectonic evolution of the Baltimore Gneiss anticlines, Maryland: Geological Society of America Special Paper 194, p. 127-148.

Newton, R.C. and Haselton, H.T., 1981, Thermodynamics of the garnet-plagioclase-Al_2SiO_5-quartz geobarometer: *in* Newton, R.C., Navrotsky, A., and Wood, B.J. (ed.) Thermodynamics of Minerals and Melts, Springer-Verlag, N.Y., p. 131-147.

Olsen, S.N., 1977, Origin of the Baltimore Gneiss migmatites at Piney Creek, Maryland: Geological Society of America Bulletin, v. 88, p. 1089-1101.

Reinhardt J. and Crowley, W.P., 1979, Geologic map of the Baltimore East Quadrangle, Maryland: Maryland Geological Survey.

Rodgers, J., 1982, The life history of a mountain range — the Appalachians: *in* Hsu, K.J. (ed.) Mountain Building Processes, Academic Press London, U.K., p. 229-241.

Sinha, A.K., 1988, Granites and gabbros - A field excursion through the Maryland Piedmont, V.M. Goldschmidt Conference, Baltimore, Maryland.

Solberg, T.N. and Speer, J.A., 1982, QALL, A 16-element analytical scheme for efficient petrologic work on an automated ARL-SEMQ: Application to mica reference samples: *In* Heinrich, K.F.J., (ed.) Microbeam Analysis — 1982, San Francisco, California, p. 422-426.

Southwick, D.L., 1968, Crystalline rocks of Harford County: *In* The Geology of Harford County, Maryland Geological Survey, p. 1-76.

Southwick, D.L. and Owens, J.P., 1968, Geologic Map of Harford County: Maryland Geological Survey.

Spear, F.S., Selverstone, J., Hickmott, D., Crowley, P. and Hodges, K.V., 1984, P-T paths from garnet zoning: A new technique for deciphering tectonic processes in crystalline terranes: Geology, v. 12, p. 87-90.

Sutter, J.F., Pavlides, L., Kunk, M.J. and Cortesini, H., Jr., 1985, Late Paleozoic metamorphism and uplift in the Piedmont near Fredericksburg, Virginia: Geological Society of America Abstracts with Programs, v. 17, p. 138.

Thomas, W.A., 1977, Evolution of Appalachian - Ouachita salients and recesses from reentrants and promontories in the continental margin: American Journal of Science, v. 277, p. 1233-1278.

Tracy, R.J. and Robinson, P., 1988, Silicate-sulfide-oxide-fluid reactions in granulite-grade pelitic rocks, central Massachusetts: American Journal of Science, v. 288-A, p. 45-74.

Tracy, R.J., Robinson, P. and Thompson, A.B., 1976, Garnet composition and zoning in the determination of temperature and pressure of metamorphism, central Massachusetts: American Mineralogist, v. 61, p. 762-775.

Vernon, R.H. and Flood, R.H., 1977, Interpretation of metamorphic

assemblages containing fibrolitic sillimanite: Contributions to Mineralogy and Petrology, v. 59, p. 227-235.
Williams, H., 1978, Tectonic lithofacies map of the Appalachian Orogen, Memorial University of Newfoundland, Map No. 1.
Williams, H. and Hatcher, R.D. Jr., 1983, Appalachian suspect terranes, Geological Society of America Memoir 158, p. 33-53.
Zen, E-an, 1981, An alternative model for the development of the allochthonous southern Appalachian Piedmont: American Journal of Science, v. 28, p. 1153-1163.

GEOLOGIC AND TOPOGRAPHIC CONTROLS ON THE RAPIDS OF THE NEW RIVER GORGE, WEST VIRGINIA

HUGH H. MILLS

Department of Earth Sciences
Tennessee Technological University
Cookeville, TN 38505

ABSTRACT

Variations in valley form, valley and channel width, gradient, maximum boulder size, channel narrowing at rapids, tributary gradient and basin area, and difficulty rating of rapids were examined over a 76-km reach of the New River Gorge. The valley cross section becomes progressively narrower and steeper walled downstream as the lower contact of the highly resistant New River Formation gradually descends toward river level. Valley and channel width decrease gradually by a factor of 2. Maximum boulder size and stream gradient show little systematic variation over the 65-km upstream reach, but increase by a factor of 3 or 4 in the final 11 km; the most difficult rapids also occur in this downstream reach. The dramatic increase in boulder size (to values exceeding 10 m) appears to stem from a combination of valley narrowing and proximity to the valley floors of resistant sandstone outcrops. Gradient is probably a function mainly of boulder size. Rating of rapids increases with steeper gradients, narrower channel widths, and larger boulders. For 15 rapids in the lower 11-km reach, difficulty rating correlates highly with the surveyed vertical drop. In contrast to rivers of the Colorado Plateau, the majority of rapids in the gorge appear to result from mass movements on the valley walls rather than from deposition at tributary mouths. Channel constriction at rapids along the New River is much less than that reported for the Colorado River. This difference may reflect the greater importance of mass movement for formation of rapids, as well as a longer recurrence interval for constricting depositional events in the Appalachian Plateau relative to the Colorado Plateau.

INTRODUCTION

The New River Gorge of West Virginia provides one of the most popular whitewater locations in the United States. Although more severe rapids can be found, the combination of challenging rapids, accessibility, and beautiful scenery is probably unequalled in the eastern United States. Each year tens of thousands of people run the reach of the gorge between Thurmond and the New River bridge. For earth scientists as well as for many nonscientists, the experience stimulates questions about the rapids. What causes rapids? Why do they occur where they do? What makes one rapid more difficult than another? Geologists, hydrologists, and physical geographers have investigated these questions for rivers of the Colorado Plateau, but rivers of the Eastern states have received little or no attention. The present study examines physical controls on the rapids and other geomorphic features of the New River Gorge in light of previous work in the Southwest, with the goal of determining just what controls the location and character of the New River rapids.

PREVIOUS WORK

Leopold (1969) considered the alternating pools and rapids of the Colorado River in the Grand Canyon to be analogous to the pools and riffles of smaller, gravel-bedded meandering streams, the spacing of which results from internal hydraulic adjustment. Dolan and others (1978), however, in a more systematic investigation, concluded that most rapids are produced by tributary debris fans that constrict the main channel. Similarly, Graf (1979) found that of 410 rapids in 12 canyon rivers of the Colorado Plateau, 278 were located at tributary mouths, 100 at mass-movement sites, and only 32 had no obvious sources of debris. Debris fans typically occur at the confluences of small rather than large tributaries (Dolan and others, 1978). Webb and others (1987, 1988) have recently demonstrated that many tributary fans may be emplaced chiefly by debris flows.

Kieffer (1985, 1989) investigated the constrictions of the main channel that occur at tributary fans. She found that at a majority of these sites along the Colorado River, the channel at its narrowest part is about half as wide as it is immediately upstream from the constriction. She hypothesized that this uniformity reflects the process of widening that takes place after an episode of deposition at the tributary mouth. High flow velocity and shear stress resulting from the initial constriction produce widening by erosion, but the widening in turn leads to a decrease in the flow velocity, thereby making further widening more difficult. Erosion ceases when the constriction becomes sufficiently wide to pass the largest flood discharges at a velocity equal to the threshold velocity for erosion. This self-regulating mechanism accounts for the observed uniformity of constriction widths.

Bedrock lithology exerts an important control on rapids. Howard and Dolan (1981) concluded that along the Colorado, the chief effect of lithology is on valley width, narrow widths being associated with outcrops of resistant rocks near river level. Valley width in turn strongly influences other stream variables, including gradient as well as the frequency of cobble bars, deep pools, tributary fans, and terraces. They divided channel reaches into four types based on lithology. Of interest is the contrast between reaches crossing crystalline bedrock and those crossing massive limestones. Although the valleys of both are narrow with steep walls, those in crystalline rock have steep gradients, whereas those in limestone have gentle gradients. This difference in gradient may reflect a difference in the supply of boulders. Boulders are plentiful in streams crossing crystalline rock, but sparse in those crossing limestone. The coarser load in the streams crossing crystalline rocks results in a steeper stream gradient.

The waves that constitute whitewater generally involve supercritical flow, in which the Froude number exceeds 1 (Kieffer, 1985, 1987). The Froude number is given by

$$Fr = u/(gD)^{0.5}, \qquad (1)$$

where u is mean flow velocity, g is the acceleration due to gravity, and D is mean depth of flow. Thus, a transition from subcritical to supercritical conditions involves either a locally decreasing depth or accelerating flow, typically both. As an example of this in rapids, large boulders on the stream bed produce shallow flow over their tops, commonly producing supercritical flow. The flow returns to a subcritical condition through a hydraulic jump, which appears as a standing wave on the downstream side of the boulder. These waves may become "washed out"

as discharge increases and water level rises. In addition, convergence of flow may accelerate velocity sufficiently to produce supercritical flow. After passing through the constriction, flow returns to subcritical via a hydraulic jump, which occurs as a wave normal to flow direction. The height and position of such waves may change with discharge. Kieffer (1987) has made a detailed study of waves in rapids; the present study is concerned not with the nature of the waves, but with conditions that produce the shallowing and convergence of flow responsible for the waves.

PHYSICAL SETTING

Study was confined to that reach of the New River in West Virginia extending from near Hinton to several kilometers below Fayette Station (near the New River bridge), where the river's waters become dammed by the Hawks Nest dam (Fig. 1). Located in the Appalachian Plateau physiographic province, the New River has carved a gorge as great as 500 m deep. At Hinton the river drains an area of 16,211 km^2, where a U.S. Geological Survey gaging station has been maintained since 1937. The mean annual discharge here is 224 m^3/s. The 10-year flood is estimated to be 4,903 m^3/s, and the 100-year flood, 9,862 m^3/s (unregulated flow). At Fayette Station the area drained is 17,751 km^2, so that any downstream changes in stream character can be ascribed only in small part, if at all, to increasing discharge. A gaging station was maintained sporadically at Fayette Station between 1878 and 1916. The largest recorded flood at either station occurred at Fayette Station in 1878, having a discharge estimated at 8,785 m^3/s. The stage of that flood was 16.2 m. The largest recorded flood at Hinton was 6,970 m^3/s in 1940, and had a stage of 5.8 m. For a given discharge, flood stages at Hinton are only about one third of those at Fayette Station, owing to the much greater width of the valley floor at Hinton.

The study reach is underlain by five major geologic formations (Fig. 1); the following discussion is from Englund and others (1977, 1982), and emphasizes geologic characteristics pertinent to landform development. The Hinton Formation (Upper Mississippian) is composed primarily of calcareous shale and siltstone. The Hinton also has sandstone and limestone beds. The formation has a maximum thickness of 290-350 m in the southern part of the study area. The most resistant member of the Hinton is the Stony Gap Sandstone, about 30 m thick, composed largely of quartzose sandstone. It forms prominent cliffs and rapids along the New River near Hinton, including Sandstone Falls. The Hinton is unconformably overlain by the Bluestone Formation (Upper Mississippian), consisting chiefly of nonresistant shales, siltstones, and limestones, with thin sandstone beds. It averages about 200 m thick. Its sole resistant member is the Glady Fork Sandstone, which ranges in composition from silty ripple-bedded sandstone to coarse conglomeratic sandstone.

Above the Bluestone is the Pocahontas Formation (Lower Pennsylvanian), consisting of interbedded sandstone, shale, coal, and underclay. Sandstone is most abundant, constituting about 70 percent of the formation. A maximum thickness of about 120 m occurs in the southern part of the area. The New River Formation (Lower Pennsylvanian) unconformably overlies the Pocahontas Formation. It varies from about 305 m thick in the southeast to about 215 m in the northwest. It is a sequence of sandstone, siltstone, shale, coal, and underclay, similar to the Pocahontas except that the quartz-pebble conglomerate and quartz-

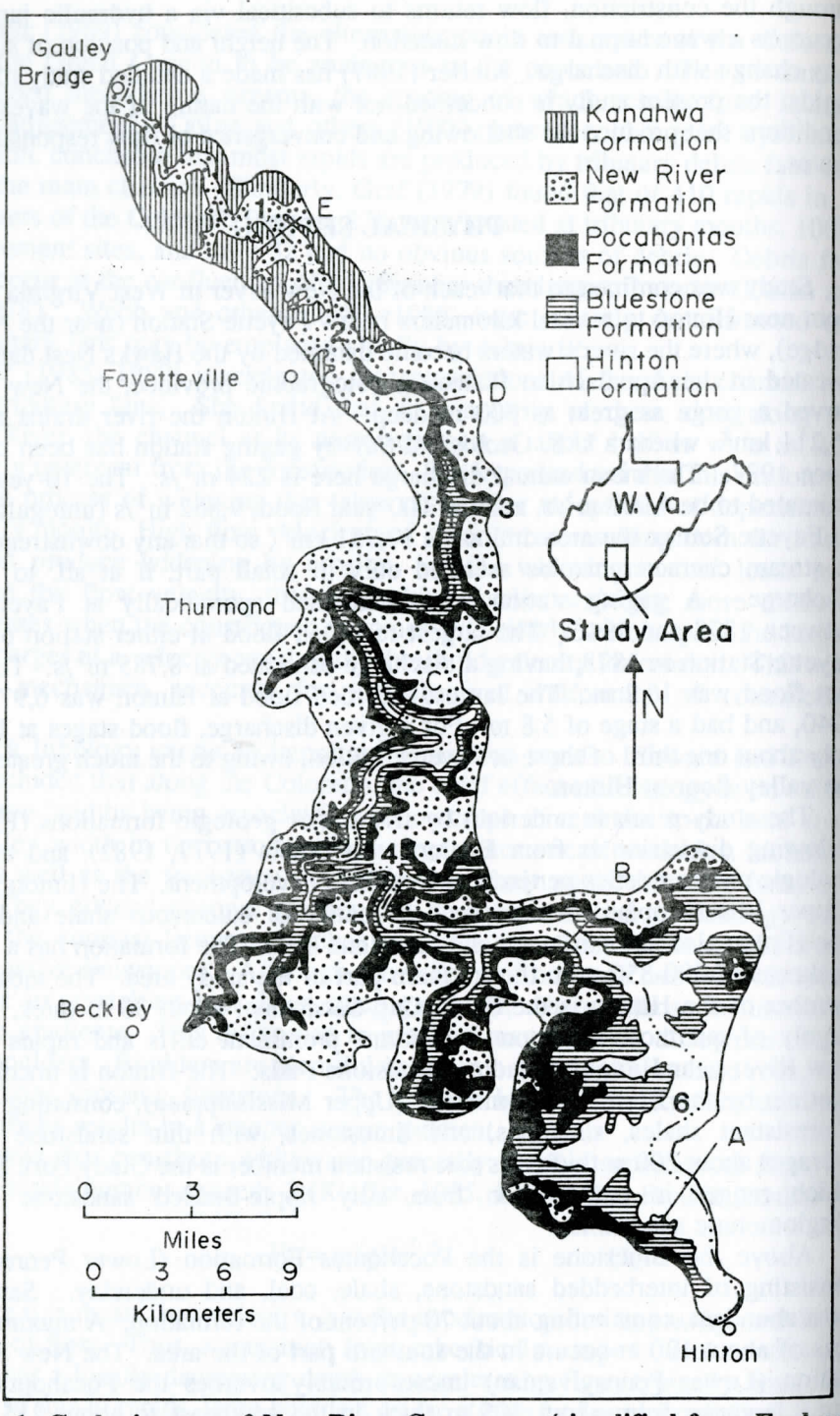

Figure 1. Geologic map of New River Gorge area (simplified from Englund and others, 1982). Lines A-E show locations of geologic cross sections in Figure 2. Numbers identify specific locations: 1) Hawks Nest dam; 2) Fayette Station and New River bridge; 3) mouth of Manns Creek; 4) Prince; 5) Grandview State Park; 6) Sandstone Falls.

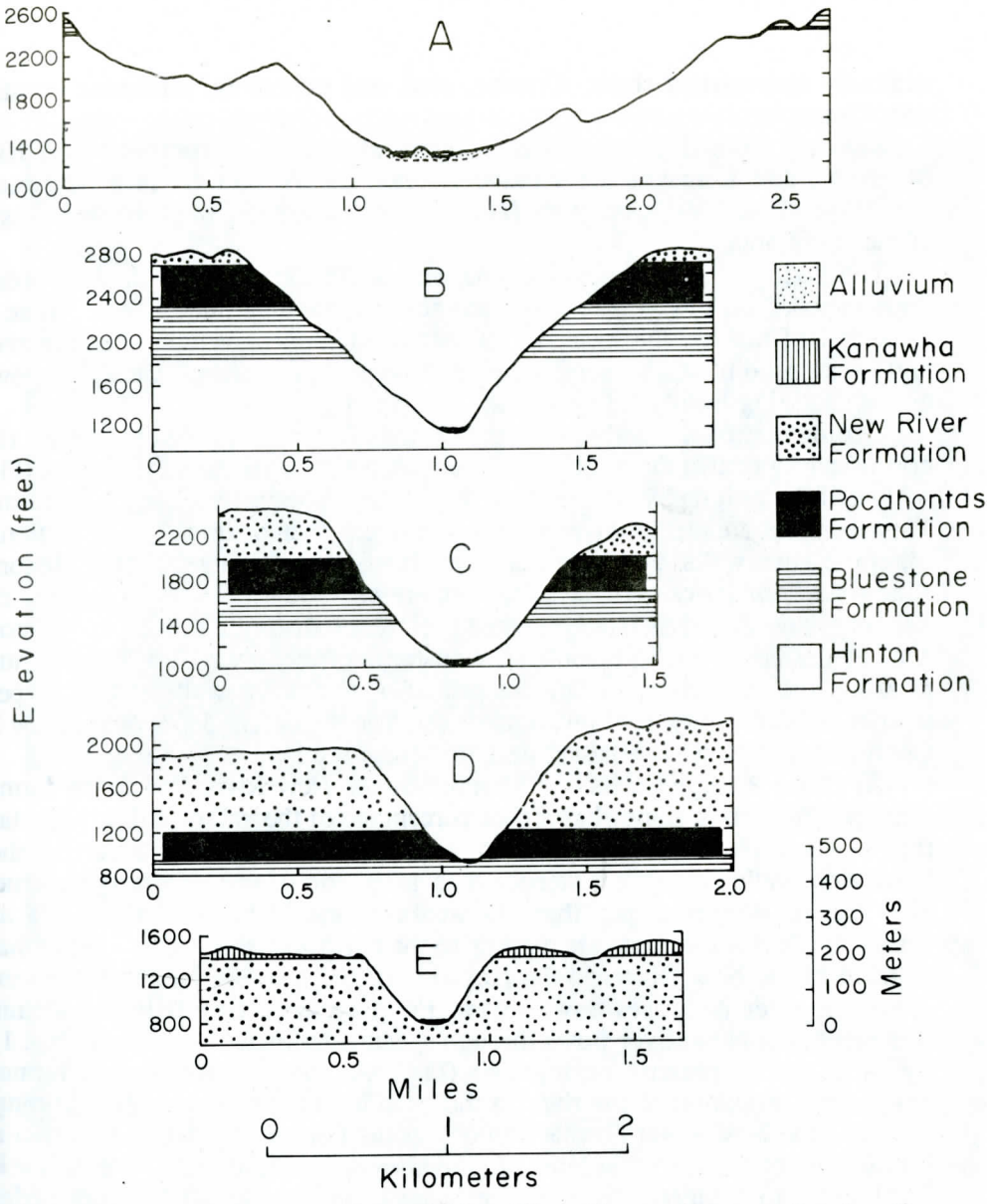

Figure 2. Geologic cross sections of New River Gorge. Cross section locations are shown on Figure 1.

ose sequences are thicker and more widespread. To the northwest, conglomeratic sandstones predominate and form high cliffs along the gorge rim. The most resistant members are the Nuttall Sandstone at the top of the formation and the Raleigh Sandstone near the middle. The topographic expression of these members becomes less conspicuous to the southeast primarily because they grade laterally to less-resistant micaceous and feldspathic sandstone with relatively low quartz content. The Kanawha Formation (Middle Pennsylvanian) is confined to the northern part of the study area, where as much as 275 m of its lower part overlies the New River Formation. About 67 percent of this formation consists of

relatively nonresistant shale, siltstone, coal, and underclay; sandstone constitutes only 33 percent.

Ranking these five formations in terms of resistance to erosion, the Hinton, Bluestone, and Kanawha are relatively weak, the Pocahontas is of intermediate strength, and the New River is by far the strongest, especially in the northwest part of the study area.

The bedrock is nearly horizontal, with a dip of about 2° to the northwest. Superimposed on this general trend are several low-amplitude folds. These have the effect of making the local dip steeper (up to 5°) or gentler than the average northwesterly dip, and in some cases reversing its direction. Faults are few and minor. Jointing locally influences the topography.

Geology strongly influences the form of the New River Gorge. On its northwesterly course the river flows over successively younger formations (Fig. 1), so that the stratigraphy of the valley walls systematically changes downstream. This change dramatically affects the valley cross section (Fig. 2). In section A of Figure 2, the walls are underlain completely by the nonresistant Hinton and Bluestone Formations. As a result, there are no strong rocks to support the rim of the gorge and the walls have retreated greatly, producing a broad valley floor and gentle sideslopes. At B, in contrast, sandstones of the lower New River Formation make up the rimrock, impeding the retreat of the valley walls so that slopes are steeper and the valley floor much narrower. The maximum depth of the New River Gorge, about 500 m, is attained near this cross section.

At C the Raleigh Sandstone Member of the New River Formation forms the rimrock. Because a somewhat higher percentage of the valley wall is underlain by the resistant New River Formation and the moderately resistant Pocahontas Formation, valley walls are steeper than at B, for stronger formations generally give rise to steeper slopes than do weaker ones. The reason for this higher percentage is that the strata are dipping to the northwest at an angle greater than the gradient of the New River, so the elevation of the resistant New River Formation above the river decreases downstream. From cross section B to the vicinity of Thurmond, the New River flows through spectacular incised meanders (Fig. 1) that typically are asymmetric or ingrown (Fig. 3A), and probably were formed by progressive migration of the river to the outside of bends during downcutting.

At D the New River Formation/Pocahontas Formation contact is within about 100 m of river level, so that most of the valley wall is underlain by the New River Formation. In addition, the highly resistant quartzose Nuttall Sandstone Member forms the rimrock. Consequently, slopes here are steeper than in any of the previous cross sections (Fig. 3B). The large incised meanders characteristic of the valley upstream do not occur here, probably because the resistant nature of the walls precludes lateral migration of meanders. The valley floor is covered with huge boulders largely derived from the Nuttall Sandstone. Because the elevation of the New River Formation has decreased still further, however, the depth of the gorge has also decreased. At E (downstream of the study reach) the New River Formation/Pocahontas Formation contact has dipped below the valley floor, so that the valley walls consist almost entirely of New River Formation. Valley walls are just as steep as at D, although the gorge is only about 185 m deep. Enormous boulders litter the valley floor.

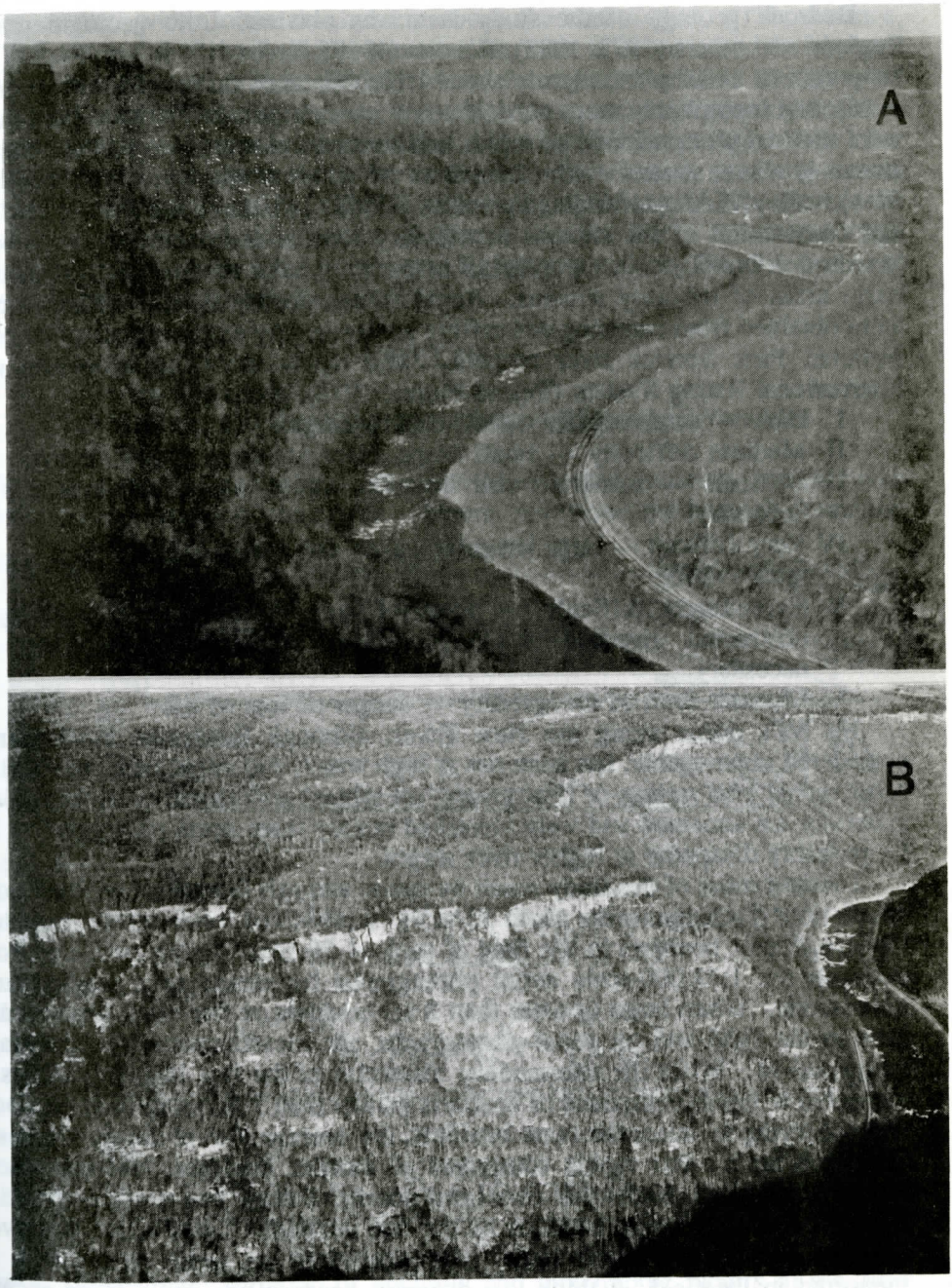

Figure 3. A. View of New River Gorge near Grandview State Park, showing typical asymmetric incised meander. Slip-off slope is to right, undercut slope to left. Relief is about 400 m. B. Aerial view of New River Gorge near cross section D. Nearly all of the valley wall is underlain by the New River Formation; the Nuttall Sandstone forms the rim, and outcrops of other sandstone units are visible. Relief is about 300 m.

PROCEDURE

Bedrock geology of the study area was obtained from geologic maps by Englund and others (1977, 1982), Hennen (1919), Krebs (1916), and Reger (1926). Low-altitude aerial photos (scale about 1:12,000, taken on July 31 and August 30, 1986), and topographic maps constructed from them for the National Park Service, were used to plot positions of rapids and to measure morphologic data, including stream gradient, stream width (defined as the width of water in the channel at low flow), valley width (defined as the valley width 30 m above the river at low flow), and constriction of the streams at tributary mouths and rapids (defined below). Standard 1:24,000-scale topographic maps were used to ascertain gradients and basin areas of tributary streams. Rapid names, locations, and difficulty ratings were obtained from canoeing and rafting guides and by extensive consultation with National Park Service river rangers. The rapids are rated according to the International Rating System (Tejada-Flores, 1978), given below:

I Easy — small regular waves, clear passages

II Medium difficulty — small drops, clear passages, routes obvious

III Difficult — numerous and irregular waves, some maneuvering necessary.

IV Very difficult — large irregular waves, fast water; calls for precise maneuvering

V Exceedingly difficult — powerful and violent water, heavily obstructed riverbed. Complex and powerful maneuvering necessary

VI Ultimate limit of navigability — danger of loss of life

No VI's occur along the New River, although Sandstone Falls, normally considered unnavigable, has been run at high water, and might be considered a VI. Most rapids with ratings of II or greater are named and appear on river guides; I's generally are unnamed and were identified mainly from aerial photographs. Many I's probably disappear at higher river stages.

I visited most of the study reach by canoe and raft in early June, 1988, during which time discharges were about 55 m^3/s. I measured intermediate diameters of the five largest boulders in the field at each of 56 sites. I also measured boulder sizes on the 1:12,000-scale aerial photographs by means of a reticle-equipped microscope. When large (greater than 3 m) boulders at one rapid were measured both in the field and on aerial photographs, the measurements generally agreed within 0.3 m. When the intermediate diameters of the five largest boulders were measured at rapids comprised of boulders greater than 3 m, using both methods but without trying to select the same boulders, the average size of the five largest still compared well. For rapids comprised of smaller boulders, however, the two methods produced results that correlated poorly. I think this result stemmed from the selection of different boulders by the two methods. I also found that average boulder size generally was larger when measured on aerial photos than when measured in the field. I think this occurred because one could more accurately find the five largest boulders on photos than in the field. In this study I therefore used the measurements from aerial photos in most cases. An exception was made for sites where the largest boulders were less than 1 m, in which case field measurements were used. Boulder sizes were measured by one or both methods at a total of 75 sites. On the reach between Manns Creek and Fayette Station, a theodolite was used to measure vertical drops at 15 rapids.

Stream constriction at rapids and tributary confluences was measured as a ratio of the low-water channel width at the narrowest part of the constriction to the greatest channel width in the reach 1 km above the constriction. (This distance, about 5-7 times the channel width, was used because in some cases the channel narrowed gradually, rather than abruptly, above the rapid.) To decide which rapids were associated with tributary mouths and which were not, the following criterion was used: a rapid was considered associated with a rapid if it occurred within 1 km downstream or 0.2 km upstream of the confluence of a tributary stream shown as perennial or intermittent on the 1:12,000-scale topographic maps. (These were the maximum upstream and downstream distances thought likely to receive large boulders carried down the tributary stream.) Rapids not meeting this criterion were considered unassociated with the tributary.

RESULTS

Relationships and Downstream Variation of Measured Variables

Figure 4 shows the downstream variation of measured variables, together with the location and ratings of the rapids. Figure 4A shows the bedrock formation

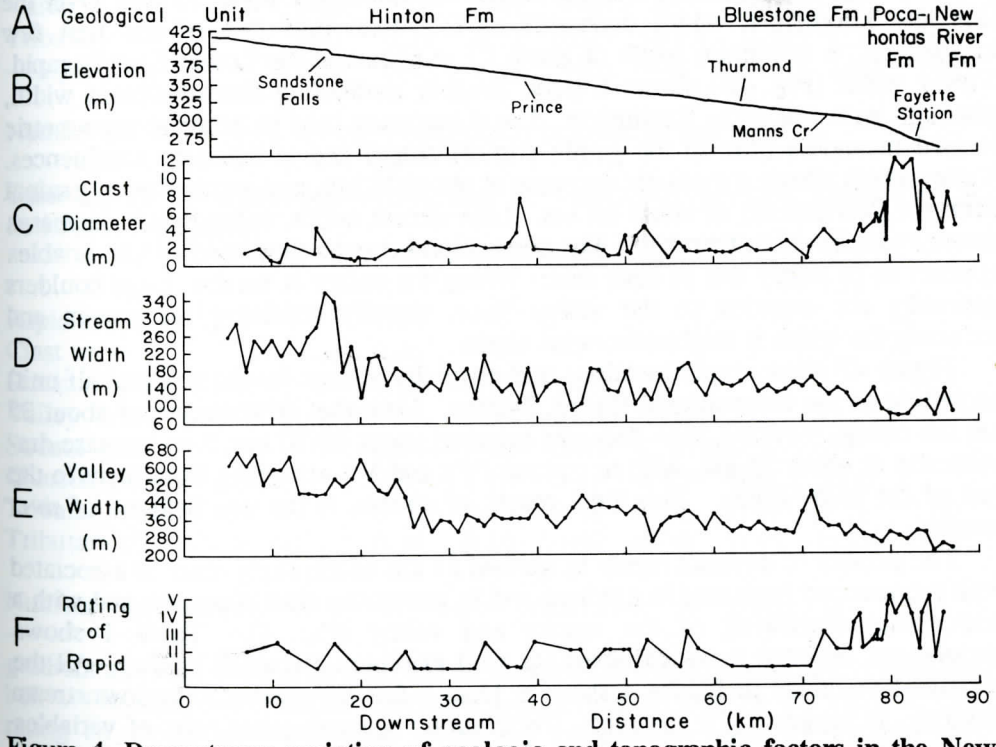

Figure 4. Downstream variation of geologic and topographic factors in the New River Gorge. A. Geologic formation at river level. B. Downstream gradient of New River (vertical exaggeration of 82X). C. Maximum clast size (mean intermediate diameter of five largest clasts). D. Stream width, measured as width of water in channel during low flow. E. Valley width, defined as width 30 m above river level at low flow. F. Rapid rating (International Rating System), to nearest half scale unit (e.g., a rating of I-II would be plotted as 1.5).

that crops out at stream level (contacts are approximate, owing to overlying Quaternary deposits and low dips of the strata). Figure 4B shows the longitudinal gradient of the New River from Bluestone dam to a point downstream of Fayette Station. Note that aside from the pronounced drop at Sandstone Falls, the gradient remains relatively constant as far as Manns Creek, then steepens dramatically. Note also that this steepening begins while the stream is flowing over the nonresistant Bluestone Formation, long before it reaches the most-resistant New River Formation.

Figure 4C shows maximum clast size, defined as the mean of the intermediate diameters of the five largest boulders at a site. This value for much of the study reach is about 2-3 m. A small increase in size occurs between 20-30 km, perhaps reflecting a lack of tributaries heading on the New River Formation upstream from this point; such tributaries have fewer boulders and lower gradients than tributaries that head on this unit. The large value at about 38 km is associated with the steep undercut slope of an asymmetric incised meander (similar to the left valley wall in Fig. 3A), and probably results from large clasts supplied by mass movement on this slope. By far the largest boulders occur along the final 11 km of the study reach; many of them are the size of small houses.

Figure 4D shows stream widths at one-km intervals along the stream. This parameter shows a decrease at about 20 km and another at about 75 km. Over the last few kilometers, width decreases to less than half that of the first few kilometers. A minimum width of about 57 m occurs at the Lower Keeney rapid. Valley width (Fig. 4E) shows a trend roughly paralleling that of stream width, although with less local fluctuation. Local increases tend to occur at asymmetric incised meanders (due to the gentle slip-off slope) and at tributary confluences. Valley width shows a dramatic decrease at about 25 km, and another more gradual decrease downstream of about 60 km. Like stream width, valley width decreases downstream by more than half. The correlation between these two width variables appears to be partly due to clast size. Where the valley is narrow, large boulders generally are supplied to the valley floor, thereby confining the stream and reducing the width it might otherwise attain.

Figure 4F shows rapid locations and difficulty ratings (to the nearest half unit) according to the International Rating System. Note that downstream of about 35 km the ratings increase, then decrease between about 60-70 km, then increase dramatically at about 75 km, with numerous IV's and V's occurring from there to the end of the study reach. This final reach, of course, is the one beloved of river runners.

The density of difficult rapids in the last 11 km of the study reach is associated with pronounced increases in gradient and in maximum clast diameter, and with a less abrupt narrowing of the stream and valley (Fig. 4). Table 1 shows correlations between these variables (as well as others discussed below). All the measured variables in Figure 4 show at least a fair correlation with downstream distance, as suggested by the plots. Correlations between other pairs of variables arise to some extent because both variables correlate with distance downstream, rather than directly with one another. This statistical effect can be removed by calculating partial-correlation coefficients (Nie and others, 1975, p. 302-305) between variables, controlling for distance downstream (Table 2). As a comparison of Table 2 with Table 1 shows, the relative strengths of correlation coefficients remain roughly the same. Of the variables discussed, the strongest correlations are between stream gradient and rapid rating and between stream

Table 1. **Correlation coefficients of measured variables.**

	DD	RR	CS	SW	VW	SG	CN	TA
Distance downstream (DD)	1.00 (76)							
Rapid rating (RR)	0.54 (58)	1.00 (58)						
Clast size (CS)	0.56 (75)	0.62 (58)	1.00 (75)					
Stream width (SW)	-0.72 (76)	-0.57 (58)	-0.50 (75)	1.00 (76)				
Valley width (VW)	-0.77 (76)	-0.37 (58)	-0.59 (75)	0.54 (76)	1.00 (76)			
Stream gradient (SG)	0.64 (76)	0.76 (58)	0.73 (75)	-0.60 (76)	-0.54 (76)	1.00 (76)		
Channel narrowing (CN)	0.02 (76)	-0.28 (58)	-0.07 (75)	0.45 (76)	-0.19 (76)	-0.07 (76)	1.00 (76)	
Tributary area (TA)	-0.05 (40)	-0.17 (40)	-0.13 (40)	-0.23 (40)	0.04 (40)	-0.11 (40)	-0.28 (40)	1.00 (40)
Tributary slope (TS)	0.47 (40)	0.52 (40)	0.62 (40)	-0.29 (40)	-0.53 (40)	0.39 (40)	0.16 (40)	-0.43 (40)

Number of values used for each correlation is given in parentheses.

Table 2. Partial-correlation coefficients of measured variables, controlling for downstream distance.

	RR	CS	SW	VW	SG	CN	TA
Rapid rating (RR)	1.00						
Clast size (CS)	0.46	1.00					
Stream width (SW)	0.31	-0.17	1.00				
Valley width (VW)	0.09	-0.30	-0.03	1.00			
Stream gradient (SG)	0.64	0.58	-0.26	-0.10	1.00		
Channel narrowing (CN)	-0.35	-0.10	0.67	-0.27	-0.11	1.00	
Tributary area (TA)	0.17	-0.12	-0.38	0.00	-0.10	-0.28	1.00
Tributary slope (TS)	0.36	0.49	0.08	-0.30	0.13	0.17	-0.46

Number of values used for each correlation is given in Table 1.

gradient and maximum clast size; the implications of these correlations is discussed below. In addition, multiple regression was performed treating the variable rapid rating as dependent. However, additional independent variables increased the variance explained by stream gradient alone only marginally.

Characteristics other than those displayed in Figure 4 also show systematic downstream changes. For example, the extent of floodplains, terraces, and islands is much greater in the upstream 15 km; as the valley and stream narrow, these features diminish in both size and extent. No large islands occur downstream of Prince. Downstream of Manns Creek, the valley floor becomes so narrow that little if any floodplain exists.

Channel Constriction Measurements

The channel narrowing ratio (CNR) was measured at the confluences of 40 tributaries. Figure 5A shows the distribution of CNR's at the confluences; the shaded areas show values measured at confluences with associated rapids, and the unshaded areas show those for confluences without rapids. The median for the first group is 0.59 and that for the second, 0.74. These values are higher than those reported by Kieffer (1985) for the Colorado River, and also more variable.

In contrast with results reported for the Colorado Plateau, of 58 rapids in the New River Gorge, only 20 occur near tributary mouths. A small part of this discrepancy results from the presence of ledge-controlled rapids; however, these occur mainly in the upstream part of the study reach and are few in number. Most rapids are associated with boulder deposits rather than ledges. Figure 5B shows CNR values for 38 rapids not associated with tributaries; the median value is 0.72.

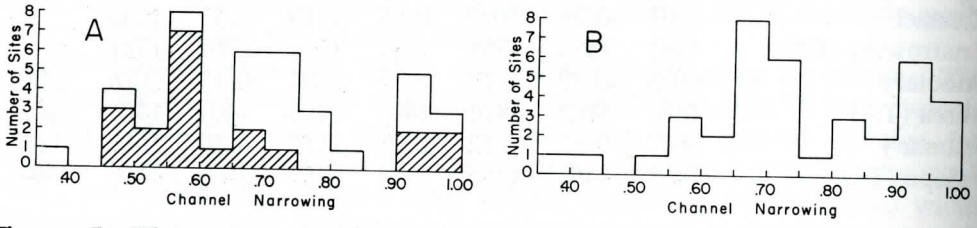

Figure 5. Histograms showing distributions of channel-narrowing ratios. A. Channel narrowing at tributary confluences. This histogram is subdivided into values for confluences with associated rapids (shaded areas) and values for confluences without associated rapids (unshaded areas). B. Channel narrowing at rapids not associated with tributary confluences.

Except for stream width, the CNR generally shows only weak correlations with other variables (Table 1). Note, in particular, that there is little relation to downstream distance. That is, even though the stream narrows downstream, the amount of constriction at individual rapids or tributary mouths is no greater downstream than upstream. There is a low but significant inverse correlation with rapid rating (partial-coefficient of –0.35). Channel narrowing at rapids thus contributes slightly to individual rapid difficulty, but it appears likely that the gradual downstream narrowing of the channel is more responsible for the high density of difficult rapids in the lower end of the study reach.

Effect of Tributary Streams

For each of the 40 tributaries considered, basin area and gradient over the final 36.6 m (120 ft) of drop were measured. Basin area of the tributaries ranged from 0.9 km^2 to 97.0 km^2. The goal was to determine whether tributary gradient or size influenced either the size of boulders in the New River or the difficulty of the rapids.

Although there is little or no downstream increase in tributary basin area, there is a moderate increase in tributary slope (Table 1). This increase probably reflects the downstream steepening of the New River Gorge walls, thereby increasing the gradient of entering tributaries. Note that tributary slope correlates more highly with

valley width than with stream width. Clast size along the New River shows a fairly high correlation with tributary slope; this might reflect a greater ability of steeper tributaries to transport large boulders to the main stream. A multiple regression of clast size on main-stream slope, tributary slope, and valley width explained 72.0 percent of the variance. Tributary basin area showed only weak correlations with other variables.

Vertical Drops and Rapid Ratings in the Lower Reach

Stream gradient, measured from 6.1-m (20-ft) contour intervals, shows a relatively high correlation with rapid rating (Tables 1 and 2). Intuitively it would seem that the actual vertical drops at individual rapids should be even a better predictor. Webb and others (1987) provided a table of difficulty ratings and vertical drops for 67 rapids along the Colorado River. Correlation of these variables produces a coefficient of 0.504 (R^2 = 25.4 percent), significant but modest.

Surveys of individual rapids are not available for the New River Gorge. So, in order to examine the correlation between the rapid rating and vertical drop, I surveyed pool-to-pool drops of 15 rapids in the 11-km stretch between Manns Creek and Fayette Station when discharge was about 55 m^3/s. For these 15 rapids, the correlation between drop and rating was 0.827 (R^2 = 0.684), much higher than for the Colorado River rapids (Fig. 6). In Figure 6, note that there is also a weaker relationship between drop and clast size (r = 0.525, R^2 = 0.276). A multiple regression of rating on vertical drop and clast size, however, showed that clast size contributed little to the predictive power of the vertical drop alone. These considerations, of course, apply only to variations within the 11-km lower reach. In explaining differences in difficulty ratings over the entire study reach, other factors, such as valley and stream width, are important.

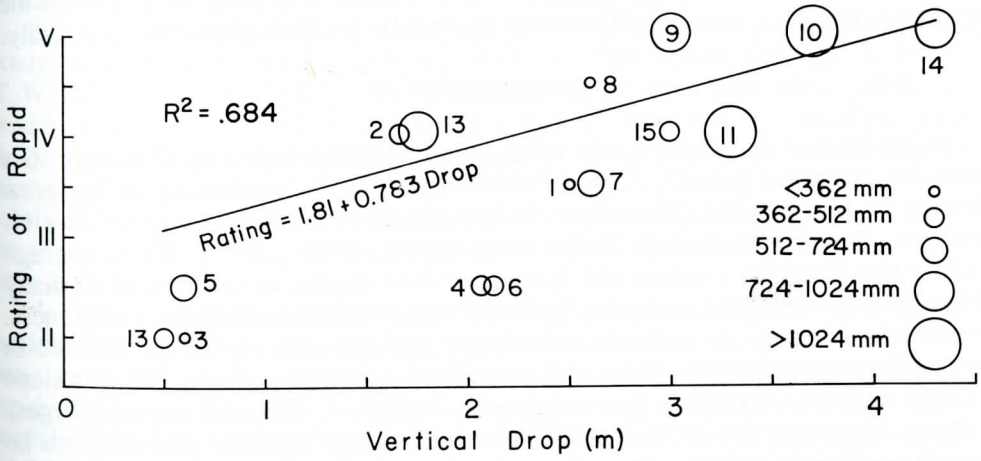

Figure 6. Plot of rapid rating against surveyed vertical drop for 15 rapids in the lower 11 kilometers of the study reach. Size of circle is proportional to maximum clast size. Rapids are as follows: 1, Upper Railroad; 2, Lower Railroad; 3, Swimmers; 4, First Warm-up (Strippers Hole); 5, Second Warm-up (Ender Waves); 6, Third Warm-up; 7, Upper Keeney; 8, Middle Keeney; 9, Lower Keeney; 10, Double Z; 11, Greyhound Bus (including Hook 99); 12, Upper Kaymoor; 13, Lower Kaymoor; 14, Undercut; 15, Fayette Station.

Boulder Transport Calculations

In ascertaining the origins of large boulders on the floor of the New River Gorge, one question to be addressed is whether the boulders could have been transported to their present positions by rare floods. A tentative answer can be obtained by applying empirical formulae to estimate competent flow depths from maximum boulder size and stream gradient, and then comparing these estimates with depths of historical floods. For example, based on 55 measurements by various authors, Williams (1983) calculated a regression equation

$$D = 0.000114\ d^{1.15}\ S^{-0.62}, \qquad (2)$$

where D is competent flow depth in meters, d is clast intermediate diameter in millimeters, and S is an approximation of the energy slope in meters/meter.

Using a slightly different set of data, Knox (1988) calculated

$$D = 0.0001\ d^{1.21}\ S^{-0.57}. \qquad (3)$$

A suitable location to apply these formulae is the Fayette Station rapids, near which a flood depth of 16.2 m was recorded in 1878, corresponding approximately to a 100-yr flood. Maximum boulder size here is 3900 mm and the gradient is 0.00386 m/m. Application of formulae (2) and (3) gives competent flow depths of 48.2 m and 52.6 m, respectively. Since these depths are about three times the depth of a 100-yr flood (and thus many times the discharge), these calculations suggest it is unlikely that boulders this large have been moved by water flows. On the other hand, under the conditions of great depths and steep energy gradients associated with very large floods in this gorge, it is possible that macroturbulent vortices may operate, making it possible to transport larger boulders than could normal tractive stresses alone (Baker, 1973). Hence, it is possible that even the largest boulders are occasionally moved by floods, but if so probably very rarely.

DISCUSSION

In the final 11 km of the study reach, stream gradient increases to three or four times its upstream value. A reasonable cause of this steepening is the great increase in boulder size that occurs in this reach. The effect of grain size on roughness is well known (e.g., Dunne and Leopold, 1978, p. 594). Where average boulder size becomes a substantial fraction of flow depths, as is the case for many of the New River rapids, grain size probably is the dominant control on roughness. In order for the river to maintain its velocity through such rapids, an increase in energy slope is necessary. Over long periods of time it is probable that this slope increase would be translated into a steeper bed gradient. (Even if the very largest boulders cannot be moved, sufficient numbers of large boulders probably can be moved to allow gradient adjustment.) Consistent with this interpretation is the relatively high statistical correlation between boulder size and gradient (Tables 1 and 2), as well as the observation by Howard and Dolan (1981) that where the Colorado River lacks large boulders in its bed, its gradient remains low even where it flows through narrow, steep-walled canyons.

An alternative interpretation is that both maximum boulder size and stream gradient are controlled by a third variable, particularly bedrock character or valley

width. However, it appears likely that the main effect of both these variables is on boulder size, with gradient being only indirectly affected. Hack (1957) observed that stream gradients in Virginia and Maryland are steeper on harder than softer bedrock, and found this effect to be due mainly to the much-larger clast sizes associated with stream reaches on hard rock. In the present setting, the increase in slope that occurs in the lower reach actually begins while the stream is still flowing on the nonresistant Bluestone Formation, but after the valley floor begins to be dominated by large blocks derived from outcrops of New River Formation sandstones on the valley wall. Similarly, the main effect of downstream narrowing of the gorge is to make it easier for large blocks from the sandstone units to reach the centerline of the valley floor.

The actual mode of transport and emplacement of large boulders at particular rapids remains problematic. Some deposits, such as the fan of larger boulders at the confluence of Wolf Creek near Fayette Station (Fig. 1), may well have been deposited by debris flows from tributaries, matrix material subsequently having been removed by floods. However, this explanation cannot be a general one, since nearly two thirds of the rapids in the gorge are not located near confluences of perennial or ephemeral streams. Boulders in some of these rapids may have been transported to the valley floors by rockfalls. At many locations, however, footslopes of the valley wall appear too gentle to allow such falls to reach the valley centerline, and a more mobile type of transport is indicated. One likely possibility is transport by debris flows generated in small ephemeral streams on valley walls which have basin areas less than 1 km^2 and slopes exceeding 20°. Examples can be seen on the left wall of Figure 3A. In the unglaciated Appalachians, thousands of debris slides have occurred in such "hollows" during historical times (Clark, 1987), although recurrence intervals at individual hollows may be in millennia (Kochel, 1987). Hundreds of hollows occur along the walls of the New River Gorge in the study reach, and most are potential sources of debris flows.

Only one recent debris slide was observed in the study area, and the presence of extensive debris-flow deposits was not obvious. This finding contrasts with that of Webb and others (1987), who found that of 36 Colorado River tributaries examined, 21 had debris-flow deposits less than 25 years old. In addition to the obscuring effect of dense vegetation, this difference may reflect greater recurrence intervals for debris flows in the Appalachian Plateau. During intervals between debris-slide events, scarred hollows become revegetated and debris-flow deposits are reworked by floods. Smaller clasts are removed, leaving only lag deposits of large boulders.

A rapid's difficulty rating is substantially determined by the more-or-less random arrangement of boulders in it, some arrangements making maneuvering of boats more difficult than others. Nevertheless, other geomorphic factors can affect rapid difficulty. Figure 7 shows the hypothesized associations of variables considered in this study. The variables most directly affecting rapid difficulty are boulder size and flow velocity. In the short term, larger boulders make flow more irregular and maneuvering more difficult, and also often contribute to large vertical drops. Greater velocity increases the extent of supercritical flow and the size of standing waves. Velocity is determined chiefly by gradient and channel width; gradient is in turn influenced, in a long-term sense, by boulder size. To a lesser extent, channel width is a function of boulder size, since banks consisting of large, relatively immobile boulders restrict channel widening.

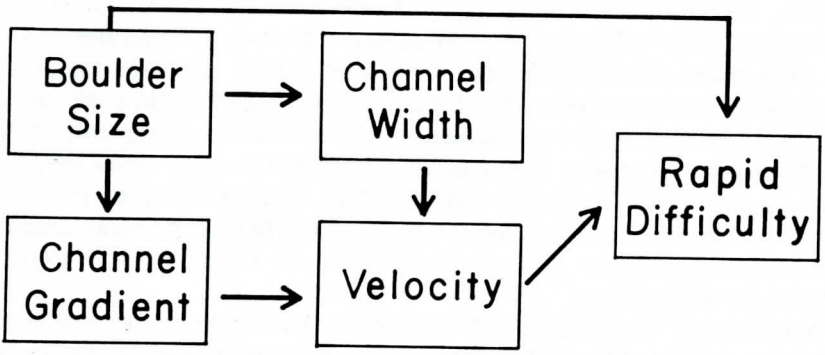

Figure 7. Diagram showing relationships of selected stream variables in the New River Gorge to one another and to rapid difficulty rating.

CONCLUSIONS

Along a 76-km reach of the New River Gorge, the valley cross section becomes progressively narrower and steeper walled downstream as thick quartzose members of the New River Formation crop out closer and closer to river level. Valley and stream width decrease downstream by more than a factor of two. Stream gradient and maximum boulder size show only small variation over much of the study reach, then increase abruptly in the lower 11 km by a factor of three or four. Difficulty ratings of rapids also increase in this lower reach. Gradient appears to be closely related to boulder size, which increases dramatically in the lower reach owing to the narrowing of the gorge and the proximity of thick-bedded, resistant sandstone outcrops. Empirical formulae for competent flow depths indicate that transport of the largest boulders by water flows would require water depths approximately 3 times that of the 100-yr flood, indicating that these boulders are only very rarely moved by floods.

Boulders probably are more commonly delivered to the valley floor by mass movement from valley walls, particularly by debris slides from steep hollows, rather than by debris flows from tributaries. This inference is supported by the fact that only 20 of 58 rapids are near the mouth of a perennial or intermittent stream. Rapid difficulty rating, to the extent that it does not depend on the random arrangement of boulders, is mainly a function of stream velocity and boulder size. Velocity in turn is mainly a function of stream gradient and channel width, with gradient, over the long term, being largely determined by boulder size.

The finding that channel-narrowing ratios at rapids are higher and more variable than those reported for the Colorado River may reflect the greater importance of mass movements from valley walls for rapid formation in the New River Gorge. The higher values may also stem from a much longer recurrence interval of events that constrict the New River channel relative to similar events in the Colorado Plateau, so that recent events are rare and most constrictions have had sufficient time to attain an equilibrium width. The low correlation of narrowing ratio with rapid rating, plus the lack of downstream change in the ratio, suggest that the general downstream narrowing of the channel contributes more to the difficulty of rapids in the lower reach than does local constriction.

ACKNOWLEDGEMENTS

Many National Park personnel from the New River Gorge National River provided help for this project, including Andy Kardos, Meg Weesner, Don Kodak, Mary Beth Maynard, Rick Brown, Mike Murray, Rob Turan, Mark Benson, and Ray O'Neil. Jon Dragan also provided helpful information. Jeff Wiley of the U.S. Geological Survey supplied hydrologic data, and Dave Furbish and Will Graf provided helpful reviews. James Hollars served ably as field assistant.

REFERENCES CITED

Baker, V.R., 1973, Paleohydrology and sedimentology of Lake Missoula flooding in eastern Washington: Geological Society of America Special Paper 144, 79 p.

Clark, G.M., 1987, Debris slide and debris flow historical events in the Appalachians south of the glacial border, *in* Costa, J.E., and Wieczorek, G.F., Debris flows/avalanches: process, recognition, and mitigation: Boulder, CO, Geological Society of America Reviews in Engineering Geology, v. 7, p. 125-138.

Dolan, R., Howard, A., and Trimble, D., 1978, Structural control of the rapids and pools of the Colorado River in the Grand Canyon: Science, v. 202, p. 629-631.

Dunne, Thomas, and Leopold, L.B., 1978, Water in environmental planning: San Francisco, Freeman and Co., 818 p.

Englund, K.J., King, E.R., Lesure, F.G., Perry, W.J., Jr., 1977, Mineral resource, geological, and geophysical maps of the New River Gorge area, Fayette, Raleigh, and Summers counties, West Virginia: U.S. Geological Survey Open-File Report 77-076, 12 sheets, 26 maps.

Englund, K.J., Johnson, P.L., and Arndt, H.H., 1982, Geology of the New River Gorge, West Virginia, *in* New River Symposium Proceedings, May 6-8, 1982, Beckley, West Virginia, p. 136-145.

Graf, W.L., 1979, Rapids in canyon rivers: Journal of Geology, v. 87, p. 533-551.

Hack, J.T., 1957, Studies of longitudinal stream profiles in Virginia and Maryland: U.S. Geological Survey Professional Paper 294-B, p. 45-97.

Hennen, R.V., 1919, Fayette County: West Virginia Geological Survey [County Report], 1002 p.

Howard, A., and Dolan, R., 1981, Geomorphology of the Colorado River in the Grand Canyon: Journal of Geology, v. 89, p. 269-298.

Kieffer, S.W., 1985, The 1983 hydraulic jump in Crystal rapid: implications for river-running and geomorphic evolution in the Grand Canyon: Journal of Geology, v. 93, p. 385-406.

Kieffer, S. W., 1987, The rapids and waves of the Colorado River, Grand Canyon, Arizona: U.S. Geological Survey Open-File Report 87-096, 74 p.

Kieffer, S. W., 1989, Geologic nozzles: Reviews of Geophysics, v. 27, p. 3-38.

Knox, J.C., 1988, Climatic influence on upper Mississippi Valley floods, *in* Baker, V.R., Kochel, R.C., and Patton, P.C., Flood geomorphology: New York, Wiley, p. 279-300.

Kochel, R.C., 1987, Holocene debris flows in central Virginia, *in* Costa, J.E., and Wieczorek, G.F., Debris flows/avalanches: process, recognition, and

mitigation: Boulder, CO, Geological Society of America Reviews in Engineering Geology, v. 7, p. 139-155.
Krebs, C.E., 1916, Raleigh County and the western portions of Mercer and Summers Counties: West Virginia Geological Survey [County Report], 778 p.
Leopold, L.B., 1969, The rapids and the pools - Grand Canyon: U.S. Geological Survey Professional Paper 669, p. 131-145.
Nie, N.H., Hull, C.H., Jenkins, J.G., Steinbrenner, K., and Bent, D.H., 1975, Statistical package for the social sciences, 2nd ed.: New York, McGraw-Hill, 675 p.
Reger, D.B., 1926, Mercer, Monroe, and Summers Counties: West Virginia Geological Survey [County Report], 963 p.
Tejada-Flores, L., 1978, Wildwater: the Sierra Club guide to kayaking and whitewater boating: San Francisco, Sierra Club Books, 329 p.
Webb, R.H., Pringle, P.T., Reneau, S.L., and Rink, G.R., 1988, Monument Creek debris flow, 1984: Implications for formations of rapids on the Colorado River in Grand Canyon National Park: Geology, v. 16, p. 50-54.
Webb, R.H., Pringle, P.T., and Rink, G.R., 1987, Debris flows from tributaries of the Colorado River, Grand Canyon National Park, Arizona: U.S. Geological Survey Open-File Report 87-118, 64 p.
Williams, G.P., 1983, Improper use of regression equations in earth sciences: Geology, v. 11, p. 195-197.